© 2020. Published by The Company of Biologists Ltd | Journal of Cell Science (2020) 133, jcs238014. doi:10.1242/jcs.238014

RESEARCH ARTICLE

SPECIAL ISSUE: CELL BIOLOGY OF THE IMMUNE SYSTEM

The Lifeact-EGFP mouse is a translationally controlled fluorescent reporter of T cell activation

Jorge Luis Galeano Niño[1,*], Szun S. Tay[1,*,‡], Jacqueline L. E. Tearle[1,*], Jianling Xie[2], Matt A. Govendir[1], Daryan Kempe[1], Jessica Mazalo[1], Alexander P. Drew[3], Feyza Colakoglu[1], Sarah K. Kummerfeld[3,4], Christopher G. Proud[2,5] and Maté Biro[1,6,‡]

ABSTRACT

It has become increasingly evident that T cell functions are subject to translational control in addition to transcriptional regulation. Here, by using live imaging of CD8$^+$ T cells isolated from the Lifeact-EGFP mouse, we show that T cells exhibit a gain in fluorescence intensity following engagement of cognate tumour target cells. The GFP signal increase is governed by Erk1/2-dependent distal T cell receptor (TCR) signalling and its magnitude correlates with IFN-γ and TNF-α production, which are hallmarks of T cell activation. Enhanced fluorescence was due to increased translation of Lifeact-EGFP protein, without an associated increase in its mRNA. Activation-induced gains in fluorescence were also observed in naïve and CD4$^+$ T cells from the Lifeact-EGFP reporter, and were readily detected by both flow cytometry and live cell microscopy. This unique, translationally controlled reporter of effector T cell activation simultaneously enables tracking of cell morphology, F-actin dynamics and activation state in individual migrating T cells. It is a valuable addition to the limited number of reporters of T cell dynamics and activation, and opens the door to studies of translational activity and heterogeneities in functional T cell responses *in situ*.

KEY WORDS: Actin, Flow cytometry, Lifeact, Live imaging, T cell activation, Translation

INTRODUCTION

Cytotoxic CD8$^+$ T lymphocytes (CTLs) mediate host protection against cancer and infection by patrolling tissues for malignant or pathogen-laden cells, which they can detect and rapidly eliminate (Gerlach et al., 2010). Central to the ability of CTLs to home to and migrate within tissues, and to engage and kill targets, is their capacity for rapid shape change, which relies on the tightly regulated remodelling of cortical networks of filamentous actin (F-actin) (Vicente-Manzanares and Sánchez-Madrid, 2004; Billadeau et al., 2007). Motile leukocytes typically display a polarised morphology characterised by actin-mediated protrusivity at the leading edge and actomyosin-dependent contractility at the rear (Weninger et al., 2014). Live cell microscopy and associated image analysis techniques, together with the development of fluorescent reporters, have enabled the study of the intricacies of leukocyte dynamics. A genetically encoded reporter based on an F-actin binding peptide fused to enhanced green fluorescent protein (Lifeact-EGFP) (Riedl et al., 2008) and its derivative transgenic reporter mouse (Riedl et al., 2010) opened the door to live imaging of cellular F-actin dynamics. Applied to T cells, it led to our understanding that during cytotoxic synapse (CS) formation with target cells, F-actin is cleared from the centre of the CS, through which the delivery of cytotoxic granules is then enabled (Ritter et al., 2015). The tracking of T cell movements and interactions, synapse formation and killing of targets (Mullins and Hansen, 2013) has led to a better understanding of the processes preceding and following T cell activation (Zhao et al., 2012). Upon cognate antigen recognition on the surface of a target cell, T cell receptor (TCR) triggering initiates a proximal signalling cascade via the recruitment of the Src family kinases Lck and Fyn (Chakraborty and Weiss, 2014), resulting in the phosphorylation of the immunoreceptor tyrosine activation motifs (ITAMs) in the cytoplasmic domains of the TCR-CD3 complex (Love and Hayes, 2010). The recruitment of Zap-70 to the ITAMs then induces a series of further phosphorylation events that drive surface receptor and integrin clustering, as well as the membrane and cytoskeletal remodelling that underpin CS formation (Kumari et al., 2014). Subsequent distal TCR signalling, mediated via phosphorylation and nuclear translocation of extracellular signal-regulated kinases (Erk1/2; also known as MAPK3 and MAPK1, respectively), induces a ‘late phase’ of T cell activation characterised by sustained secretion of pro-inflammatory cytokines such as interleukin 2 (IL-2), IL-22 and interferon gamma (IFN-γ) (Yeh et al., 2008). Proximal TCR signalling and early phase T cell activation is completed within the first 15 min of antigen encounter (Varma et al., 2006), whereas late phase activation takes place over several hours (2-6 h) and governs the long-term immune response of effector T cells (Koike et al., 2003).

In addition to phosphorylation-mediated signalling cascades, such as those downstream of TCR triggering, evidence suggests that important facets of leukocyte activation are specifically subject to translational control, which accelerates the delivery of effector functions. For instance, the rapid and targeted translation of cytokines in primed T cells following antigen re-encounter restricts potent effector cytokine production to intended target sites (Piccirillo et al., 2014). Moreover, natural killer (NK) cells acquire cytotoxic functions by translating pre-existing pools of perforin and granzyme B mRNA transcripts (Fehniger et al., 2007). Translational control has recently been shown to be important for timely induction and resolution of inflammation through

[1]EMBL Australia, Single Molecule Science Node, School of Medical Sciences, University of New South Wales, Sydney, NSW 2052, Australia. [2]Lifelong Health Theme, South Australian Health and Medical Research Institute, North Terrace, Adelaide, SA 5000, Australia. [3]Kinghorn Centre for Clinical Genomics, Garvan Institute of Medical Research, Sydney, NSW, Australia. [4]St Vincent’s Clinical School, University of New South Wales, Sydney, NSW, Australia. [5]School of Biological Sciences, University of Adelaide, Frome Road, Adelaide. [6]ARC Centre of Excellence in Advanced Molecular Imaging, University of New South Wales, Sydney, NSW 2052, Australia.
*These authors contributed equally to this work

‡Authors for correspondence (s.tay@unsw.edu.au; m.biro@unsw.edu.au)

S.S.T., 0000-0003-0186-8154; M.B., 0000-0001-5852-3726

Received 20 August 2019; Accepted 4 February 2020

Journal of Cell Science (2020) 133, jcs238014. doi:10.1242/jcs.238014

translatome analyses of macrophage (Schott et al., 2014), naïve T cell (Tan et al., 2017) or effector T cell maturation and activation (Araki et al., 2017), which all reveal complex specificities beyond global protein synthesis in how cellular programs are induced by translational discrimination. For instance, naïve $CD8^+$ T cells prioritise translation of transcripts required for ribosome biogenesis to ensure ribosome sufficiency (Tan et al., 2017), whilst CTLs engage both translational upregulation and suppression mechanisms as they progress from the clonal expansion phase to contraction phase (Araki et al., 2017). Distinct subsets of $CD4^+$ T regulatory cells can also be distinguished by their translatomes (Bjur et al., 2013).

Here, we reveal that, following activation, $CD4^+$ and $CD8^+$ T cells isolated from the widely adopted Lifeact-EGFP reporter mouse exhibit a marked increase in fluorescence (hereafter also simply 'GFP') that is readily detected by flow cytometry and fluorescence microscopy. The increased fluorescence correlates with interferon gamma (IFN-γ) and tumor necrosis factor (TNF-α; now known as TNF) production and late phase T cell activation, and is translationally controlled via the mTOR pathway. Our results indicate that the Lifeact-EGFP mouse is a valuable simultaneous reporter for F-actin dynamics, T cell activation and ensuing translational activity, allowing researchers to identify and track comprehensive T cell effector activity *in situ*.

RESULTS

Primary Lifeact-EGFP T cells exhibit a marked increase in fluorescence following interaction with cognate tumour cells

To study the migratory search characteristics and killing kinetics of CTLs, we crossed Lifeact-EGFP mice to OT-I TCR transgenic mice (Hogquist et al., 1994) and co-embedded effector $CD8^+$ T cells isolated from these mice (hereafter LGO1) in 3-dimensional (3D) collagen matrices with either cognate or non-cognate EL-4 tumour cells for live imaging, as previously described (Galeano Niño et al., 2016). The addition of propidium iodide (PI) to the bathing medium allowed for the identification of lysed target cells (Jenkins et al., 2015). Combined, these methods constitute a quantitative real-time 'search-and-kill' assay, which revealed that CTLs interacting with cognate tumour cells increased in GFP fluorescence over time, but not in a non-cognate context (Fig. 1A,B; Movie 1). Statistical divergence analysis (see Materials and Methods) showed that the gain in GFP signal in T cell populations co-embedded with cognate tumour cells compared with those interacting with non-cognate cells became significant at a population level on an average of 3.7±1.1 h after co-embedding (Fig. 1C; Fig. S1A). The gain in GFP fluorescence was accompanied by increased migratory arrest of the T cell population (Fig. 1D) and specific clearance of cognate tumour targets (Fig. 1E, Fig. S1B, see Materials and Methods).

The increase in GFP fluorescence in LGO1 T cells following clearance of cognate tumour was also confirmed by flow cytometry (Fig. 1F, Fig. S1C), which further revealed increased granularity (side scatter area, SSC-A) and cell size (forward scatter area, FSC-A), indicative of T cell activation (Fig. S1D) (Malik et al., 2009; Pollizzi et al., 2015). No increase in GFP, SSC-A or FSC-A parameters was observed upon co-incubation with non-cognate targets (Fig. S1C,D). LGO1 T cells activated by prior co-incubation with cognate tumour cells maintained their enhanced GFP fluorescence (Fig. 1G) and a state of migratory arrest (Fig. S1E) for at least 14 h after they were sorted and re-embedded in matrices in the absence of tumour cells.

We next monitored the GFP fluorescence of LGO1 T cells during differentiation. Naïve $CD8^+$ LGO1 T cells experienced a pronounced (almost 20-fold) increase in GFP fluorescence upon stimulation, reaching a peak 48 h after primary activation by cognate peptide (Fig. 1H). The fluorescence signal then decayed over the following days but was nevertheless maintained at levels 5-fold above that of naïve T cells. At day 6, when re-stimulated with cognate tumour cells, effector LGO1 T cells again increased in GFP fluorescence (~3-fold from the elevated effector level), which was sustained for a further 48 h (Fig. 1H).

The gain in Lifeact-EGFP fluorescence is correlated with late phase T cell activation

To determine whether the gain in Lifeact-EGFP fluorescence upon activation is a result of proximal or distal TCR signalling, we employed a pan-Src family kinase (Hanke et al., 1996) and an Lck inhibitor (Seo et al., 2017), or an inhibitor of Mek1/2 (also known as MAP2K1/2) (Favata et al., 1998), the immediate upstream kinase of Erk1/2, respectively. Proximal TCR signalling was assessed by measurement of Zap-70 phosphorylation (Wang et al., 2010), which was abrogated by inhibition of Src family kinase and Lck, but not Erk1/2 (Fig. S2A). Distal TCR signalling was assessed by measurement of Erk1/2 phosphorylation, which was abrogated by Src family kinase, Lck and Erk1/2 inhibition (Fig. S2A). Therefore, the Mek1/2 inhibitor affords a specific inhibition of the distal TCR signalling pathway without compromising the proximal component, whereas Lck inhibition results in the abrogation of both.

Within the 3D search-and-kill assay, both the increase in Lifeact-EGFP signal and target clearance were abolished by Lck and Mek1/2 inhibitors (Fig. 2A,B; Fig. S2B; Movie 2), suggesting that these functions are triggered downstream of Erk1/2 phosphorylation during distal TCR signalling, consistent with the observed average lag time of 3.7 h prior to GFP increase. Interestingly, although target clearance is initiated without a lag (Fig. 2B), CTLs stop migrating under Mek1/2 inhibition to an even greater degree than control cells (Fig. S2C), suggesting that cognate contacts are still formed with targets when distal TCR signalling is inhibited. It is unclear if increased migratory arrest was due to direct inhibition of motility and adhesion, or to inhibition of cytotoxic function, leading to prolonged interactions as a result of failed disengagement (Jenkins et al., 2015), or both, resulting in reduced overall serial killing.

In an *in vitro* cytotoxicity assay where CTLs and target cells were co-pelleted at a 1:1 ratio, the inhibition of proximal TCR signalling abolished the gain in Lifeact-EGFP fluorescence (Fig. 2C) and cytotoxicity (Fig. 2D). However, whilst inhibition of distal TCR signalling significantly impaired these functions, complete abrogation was not observed. Multiple signalling cascades are activated upon TCR engagement, whereby distinct signalosomes and second messengers allow diversification of the proximal TCR signals, enabling T cells to calibrate their activation thresholds and to tune functional and proliferative responses (Gorentla and Zhong, 2012). The differential dependence on Erk1/2 signalling in the two assays could be due to higher effective antigen doses being received per CTL under static conditions, where multiple and sustained contacts are made with each target, compared with when each CTL migrates and interacts with only one or very few targets before effecting a kill in 3D collagen matrices. Nonetheless, these results highlight that the search-and-kill assay can be used to reveal distinct signalling requirements of the discrete cellular events, including migration, polarisation, scanning, migratory arrest and killing, which all contribute to overall efficacy of tumour target clearance.

To determine if the fluorescence intensity of Lifeact-EGFP T cells directly correlates with, and can therefore be used as a quantitative proxy of, the extent of T cell activation, we measured

Journal of Cell Science (2020) 133, jcs238014. doi:10.1242/jcs.238014

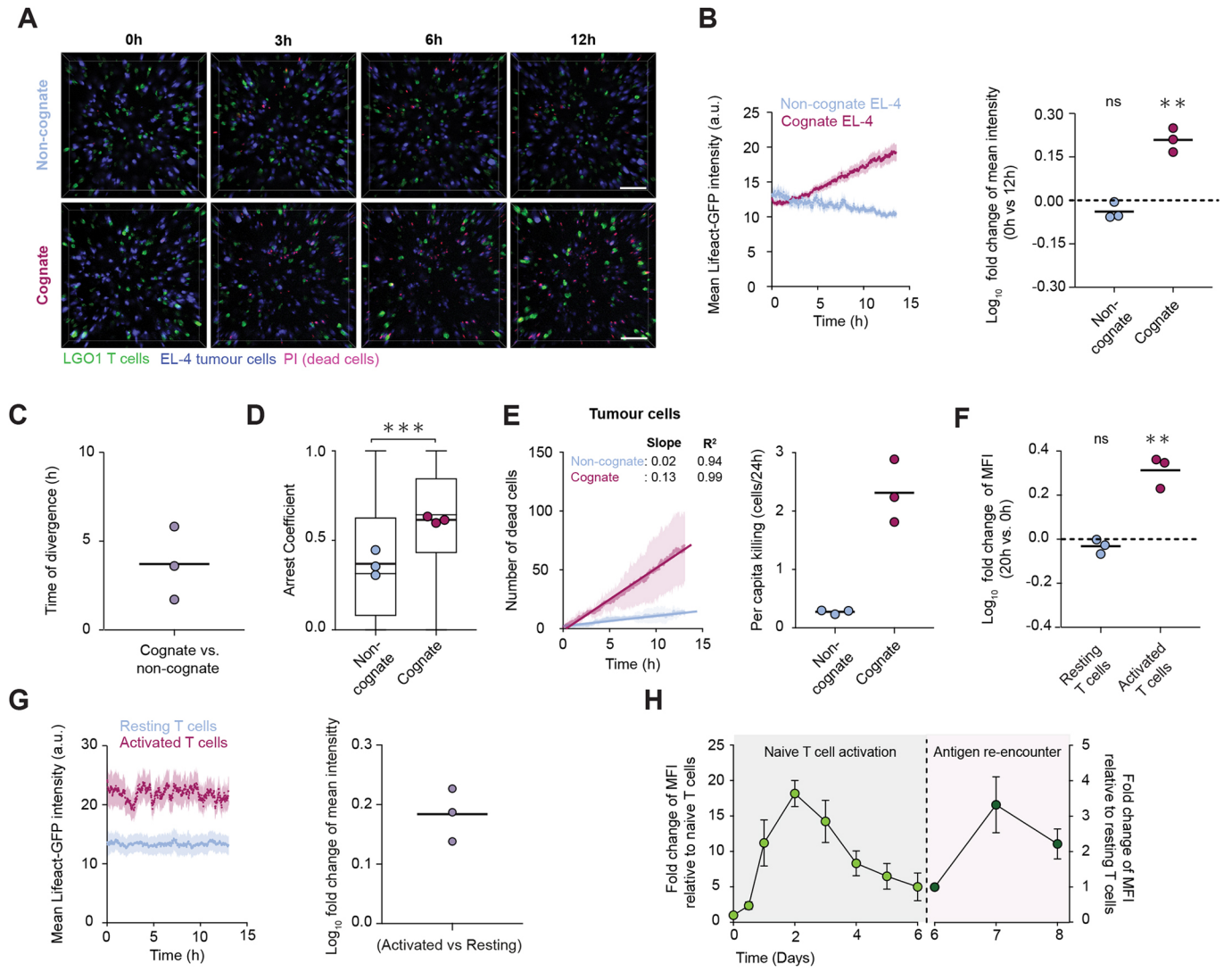

Fig. 1. CD8$^+$ T cells from Lifeact-EGFP mice exhibit a gain in fluorescence following interaction with cognate tumour cells. (A) Maximum intensity projections of live-imaged LGO1 cells (green) co-embedded in 3D collagen matrices with equal numbers of non-cognate (top row) or cognate (bottom row) EL4 tumour cells (blue). Propidium iodide (PI) in the medium identifies dying cells (red) during the experiment. Scale bars: 100 µm; representative of 3 independent experiments. (B) Population mean GFP intensities of LGO1 cells co-embedded with cognate (n=722 T cells) or non-cognate (n=650 T cells) EL4 cells from imaging performed as described in A, expressed as intensities over time (left; error bars: 95% confidence interval) or fold change at 12 h compared to 0 h [right; bars: mean. ns: P>0.05 and **P<0.01 by one sample t-test compared with a hypothetical test value of 0 (dashed line)]. (C) Time of divergence between population mean GFP intensities of LGO1 cells co-embedded with cognate or non-cognate EL4 cells[a], determined by a non-parametric right-tailed Wilcoxon rank sum test (P<0.001). (D) Distribution of the arrest coefficient of LGO1 cells. Data points: mean arrest coefficients of each independent experiment. Box-whiskers: medians and quartiles from 3 independent experiments. Thick bars: means of pooled data; ***P<0.001 by Mann–Whitney test. (E) Number of tracked PI surfaces ascribed to EL4 target cells (left) and the per capita killing rates (numbers of killed EL4 per 24 h) (right; bars: mean) from 3 independent experiments. (C-E) data pooled from 3 independent experiments performed as in A, with LGO1 cells co-embedded with cognate (n=1866 T cells) or non-cognate (n=2024 T cells) EL4 tumour cells. (F) Change in GFP mean fluorescence intensity (MFI) quantified by flow cytometry after 20 h co-culture of LGO1 cells with cognate or non-cognate EL4 cells. Bars: means of 3 independent experiments. ns: P>0.05 and **P<0.01 by one-sample t-test compared with a hypothetical test value of 0 (dashed line). (G) Population mean GFP intensities of sorted LGO1 cells re-embedded in collagen matrices without tumour cells after being co-cultured with cognate or non-cognate EL4 cells for 12 h (n=785 activated T cells, n=407 resting T cells), assessed by live imaging. GFP intensities over time (left; error bars: 95% confidence interval) and changes in intensities of activated T cells relative to resting T cells (right). Representative of 3 independent experiments. (H) Change in GFP MFI in naïve LGO1 cells stimulated with cognate peptide (SIINFEKL) relative to GFP MFI of unstimulated cells, monitored daily by flow cytometry. Antigen-experienced LGO1 cells were co-cultured with cognate EL-4 cells on day 6 and the change in fluorescence expressed relative to their resting counterparts co-cultured with non-cognate EL4. Data points: mean; error bars: s.d. of 3 independent experiments.

the production of the effector cytokines TNF-α and IFN-γ by activated T cells, which are widely adopted gold standard measures of T cell activation (Brown et al., 2017). In the *in vitro* cytotoxicity assay, IFN-γ and TNF-α secretion followed the same trend as GFP fluorescence gain and cytotoxicity upon proximal and distal TCR inhibition (Fig. 2E). On a per-cell basis, intracellular cytokine staining revealed that intracellular IFN-γ and TNF-α levels were directly correlated with Lifeact-EGFP fluorescence intensity (Fig. 2F; Fig. S2D,E). We also sorted resting and activated LGO1 CTLs into three subpopulations (high, medium and low) based on their GFP intensity (see Materials and Methods and Fig. S2F) and measured the secretion of IFN-γ and TNF-α from each subpopulation. The GFP fluorescence intensity of each subpopulation of activated LGO1 cells correlated with their levels

Journal of Cell Science (2020) 133, jcs238014. doi:10.1242/jcs.238014

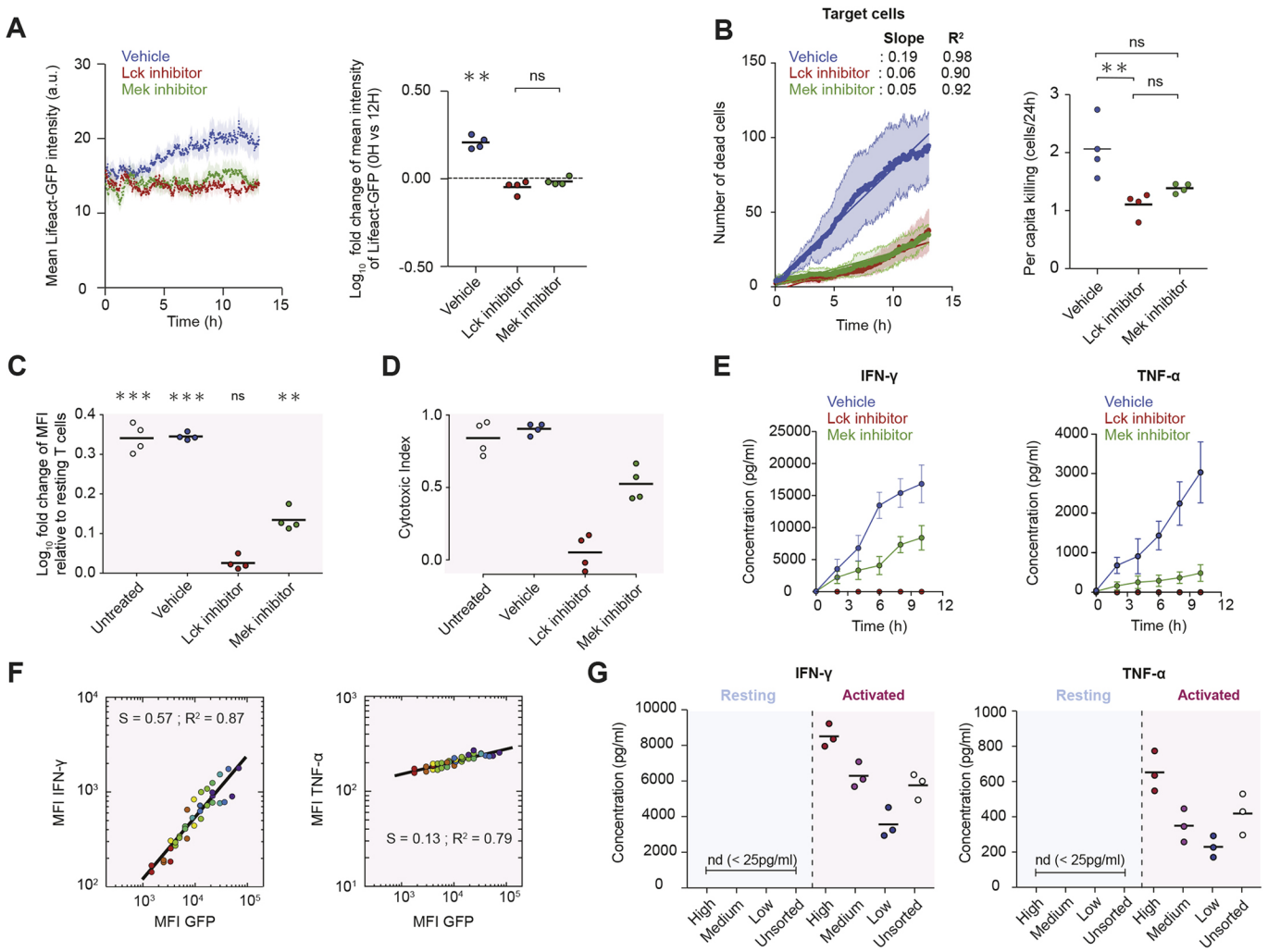

Fig. 2. Gain in GFP fluorescence of LGO1 cells is TCR mediated and is correlated with the degree of T cell activation. (A) Population mean GFP intensities of LGO1 cells co-embedded with equal numbers of cognate EL4 tumour cells in collagen matrices in the presence of inhibitors of TCR signalling (left; error bars: 95% confidence interval) and the change in mean GFP intensities at 12 h compared to 0 h [right; bars: mean. $P>0.05$ (ns) and $^{**}P<0.01$ by one-sample *t*-test compared with a hypothetical test value of 0 (dashed line)]. Live imaging data from 340 Lck inhibitor-, 268 Mek1/2 inhibitor- and 453 vehicle-treated T cells, from 4 independent experiments. (B) Number of tracked PI surfaces ascribed to EL4 cells co-embedded with LGO1 cells in the presence of TCR signalling inhibitors or vehicle as described in A (left; insert indicates slope and R^2 values of linear regression) and the per-capita killing rates (right; bars: mean of 4 independent experiments; ns: $P>0.05$ and $^{**}P<0.01$ by Kruskal–Wallis test followed by Dunn's multiple comparison test). Pooled data from 4 independent experiments. (C) Change in the GFP MFI of LGO1 cells co-cultured with cognate EL4 cells relative to fluorescence of LGO1 cells co-cultured with non-cognate EL4 cells in the presence of inhibitors of TCR signalling, measured flow cytometry. Data from 4 independent experiments. Bar, mean. ns: $P>0.05$, $^{**}P<0.01$ and $^{***}P<0.001$ by one sample *t*-test compared with a hypothetical test value of 0 (dashed line). (D) Flow cytometric quantification of the cytotoxic index of LGO1 cells co-cultured with equal numbers of cognate and non-cognate EL4 cells for 3 h in the presence of TCR signalling inhibitors or vehicle. Bar: mean of pooled data from 4 independent experiments. (E) Amount of IFN-γ and TNF-α secreted into supernatants of LGO1 co-cultures with cognate tumour EL4 cells in the presence of the TCR signalling inhibitors or vehicle, collected every 2 h over a period of 10 h. Data points: mean from 3 independent experiments; error bars: standard deviation. (F) MFI of IFN-γ or TNF-α detected by intracellular cytokine staining, correlated to the MFI of Lifeact-GFP in activated LGO1 cells. S, slope; R^2, coefficient of correlation. (G) Amount of IFN-γ and TNF-α secreted by LGO1 cells of high, medium and low GFP intensity sorted according to the gates defined in Fig. S2F after they had been co-cultured with non-cognate (resting) or cognate (activated) EL4 cells for 12 h. Bars: mean of 3 independent experiments; nd: not detected.

of secretion of both cytokines (Fig. 2G), with an activated but unsorted population yielding intermediate levels of cytokine secretion (Fig. 2G). By contrast, increases in cell size, as determined by the FSC-A parameter in flow cytometry (Malik et al., 2009; Pollizzi et al., 2015; Jenkins et al., 2015), was indistinguishable between the three subpopulations (Fig. S2F), indicating that the magnitude of the gain in Lifeact-EGFP fluorescence cannot be accounted for simply by an increase in T cell size upon activation (Fig. S2F). Thus, the gain in Lifeact-EGFP fluorescence upon activation: (1) is governed by distal TCR signalling; (2) strongly correlates with IFN-γ and TNF-α production; and (3) serves as a better discriminator of the level of activation in T cell subpopulations within an activated cohort than cell size.

The specific Lifeact-EGFP fluorescence increase upon T cell activation is translationally regulated

The activation-induced increase in fluorescence is not observable in effector T cells isolated from fluorescent reporters other than Lifeact-EGFP. Neither tdTomato nor GFP intensities, from the TCR-transgenic mG/mT×OT-I and UBC-GFP×gBT-I reporter mice, respectively (see Materials and Methods), increased

Journal of Cell Science (2020) 133, jcs238014. doi:10.1242/jcs.238014

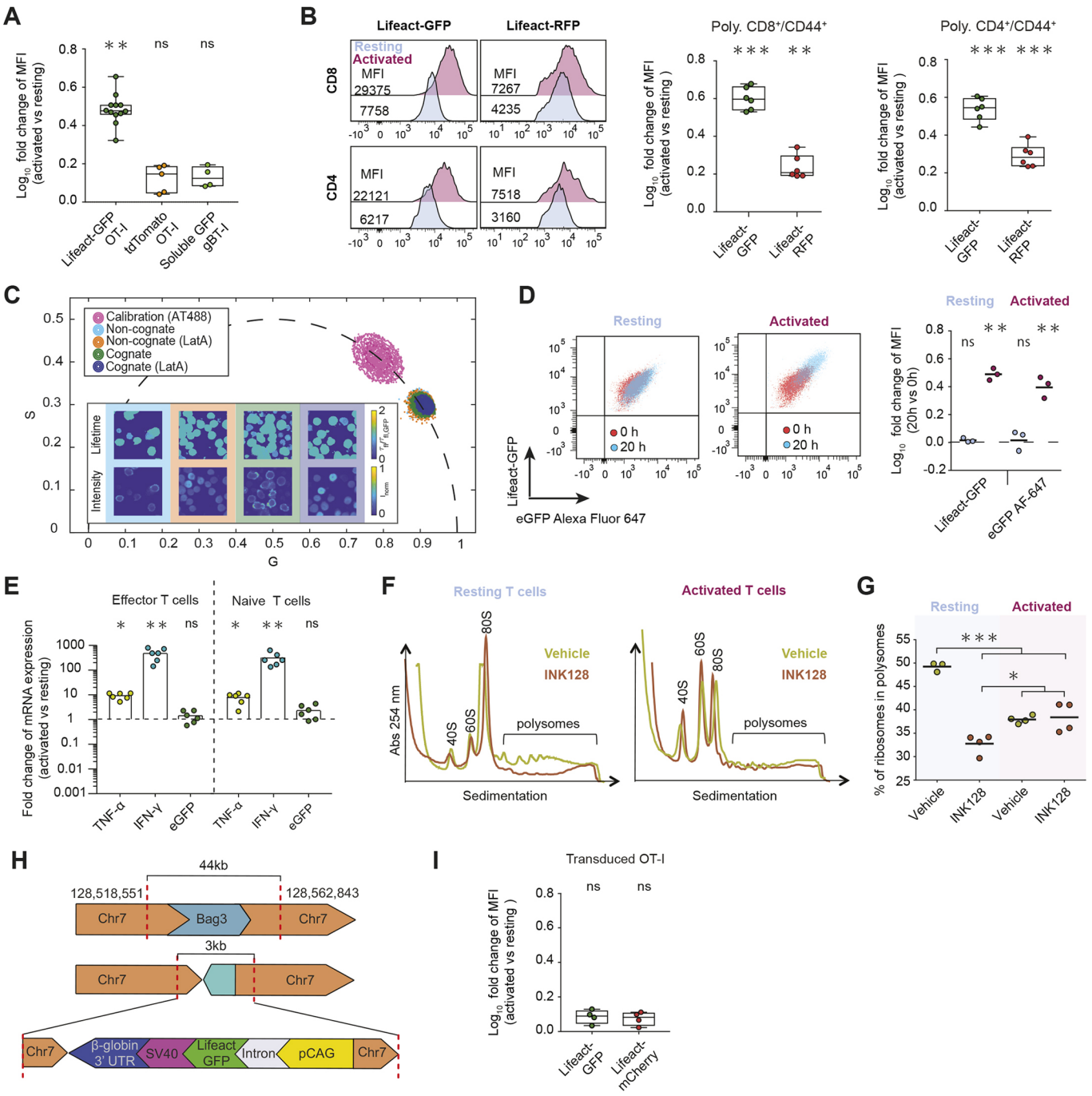

Fig. 3. See next page for legend.

significantly in CTLs activated by cognate tumour targets compared with their resting counterparts (Fig. 3A). Therefore, overall increase in protein synthesis upon T cell activation cannot solely account for the gain in fluorescence in activated LGO1 T cells. We then generated polyclonal CD4$^+$ and CD8$^+$ effector T cells from non-TCR transgenic Lifeact-EGFP and Lifeact-mRFPruby (hereafter Lifeact-RFP) mice, and stimulated these with anti-CD3/anti-CD28-coated beads. Both CD4$^+$ and CD8$^+$ T cells from the Lifeact-EGFP mice displayed a marked increase in fluorescence upon activation, whereas the gain in Lifeact-RFP was far less pronounced (Fig. 3B), despite comparable levels of TCR-mediated activation indicated by the magnitude of TCR-Vα downregulation (Fig. S3A). The stronger activation signal conferred by beads compared with cellular targets likely accounts for the slight increase in fluorescence in the Lifeact-RFP T cells, which remains far lower than in Lifeact-EGFP T cells.

We then investigated whether the increase in Lifeact-EGFP fluorescence could be due to a greater abundance of either total or filamentous actin. Activated T cells have previously been reported to globally assemble more F-actin than resting cells when evaluated by flow cytometry (Kim et al., 2009). We measured no significant increase in either Phalloidin or total β-actin staining in activated T cells compared with resting T cells (Fig. S3B), nor did we detect increased mRNA levels for β- or γ-actin (Fig. S3C). Upon complete depolymerisation of the F-actin network following latrunculin A

Fig. 3. Increased Lifeact-GFP fluorescence and protein is translationally regulated and is unique to the Lifeact-eGFP reporter mouse. (A) Changes in MFI of LGO1, mG/mT.OT-I or UBI-GFP.gBT-I activated or resting TCR transgenic T cells co-cultured for 20 h with the cognate peptide-pulsed or non-cognate EL4 cells, relative to the fluorescence of the corresponding resting T cells, measured by flow cytometry. Box-whiskers: medians and quartiles of the pooled data from at least 4 independent experiments. ns: $P>0.05$ and $^{**}P<0.01$ by one sample *t*-test compared with a hypothetical test value of 0. (B) LifeactGFP or RFP fluorescence in polyclonal $CD8^+/CD44^+$ or $CD4^+/CD44^+$ T cells isolated from Lifeact-EGFP and Lifeact-RFP mice stimulated for 20 h with streptavidin beads coated with biotinylated CD3/CD28 antibodies (activated) or with IgG isotype control (resting). Representative flow cytometry histograms (left) and change in fluorescence intensities of activated relative to resting cells of 6 independent experiments (right) are shown. Box-whiskers: medians and quartiles of the pooled data from 6 independent experiments. ns: $P>0.05$ and $^{**}P<0.01$ by one sample *t*-test compared with a hypothetical test value of 0. (C) Phasor 2D histogram of FLIM analysis of Lifeact-GFP in LGO1 cells co-cultured with either cognate or non-cognate EL4 cells for 20 h, with LatA treatment for an additional 30 min. The G-S pair densities from three different fields of view are displayed as isocontours. ATTO 488 NHS-Ester was used as calibration standard. In inset, frames are colour-coded according to main figure, showing representative FLIM images of the fluorescence lifetime per pixel normalized to the fluorescence lifetime of GFP (2.7 ns) (top) and representative images of the fluorescence intensity per pixel normalized to the maximum per-pixel-intensity across the four images (bottom). (D) Intracellular eGFP expression detected using an Alexa Flour 647-conjugated anti-GFP antibody versus intrinsic Lifeact-GFP fluorescence in activated or resting LGO1 cells after co-culture with cognate or non-EL4 cells, respectively, measured by flow cytometry. Representative plots (left and middle) and the changes in Lifeact-GFP and Alexa Flour 647 intensities at 20 h compared to 0 h (right). Bar: mean of pooled data from 3 independent experiments. ns: $P>0.05$ and $^{**}P<0.01$ by one-sample *t*-test compared with a hypothetical test value of 0 (dashed line). (E) TNF-α, IFN-γ and eGFP mRNA expression in activated or resting effector and naïve LGO1 cells sorted after co-culture with cognate or non-cognate EL4 cells for 12 h, respectively; normalised to genes encoding housekeeping proteins RPL13A and β2M. Bar: mean of pooled data from 6 independent experiments. ns: $P>0.05$, $^{*}P<0.05$ and $^{**}P<0.01$ by one-sample *t*-test compared with a hypothetical test value of 0 (dashed line). (F) Polysome profiles of resting (left) or activated (right) LGO1 cells co-cultured with non-cognate or cognate EL4, respectively, in presence of INK128 (1 µM) or vehicle for 20 h before sucrose gradient fractionation and quantification of absorbance (at 254 nm). (G) Percentage of ribosomes engaged in polysomal fractions (fractions 6-10) in resting or activated LGO1 cells in the presence of INK128 (1 µM) or vehicle. Bar: mean of pooled data from 4 independent experiments. $^{*}P>0.05$ and $^{***}P<0.001$ by one-way ANOVA following Tukey's multiple comparison test. (H) Schematic showing the site of insertion of the Lifeact-GFP transgene. A 44,292 bp deletion that includes the BAG3 gene (23,365 bp, NCBI gene ID 29810) occurred at the site of Lifeact-EGFP insertion in chromosome 7 (top; positions indicated). A single copy of the Lifeact-EGFP transgene (3268 bp) was inserted in the reverse direction (middle). Features in the transgene include the pCAG promoter (1772 bp, yellow), 5′ intron splice site (12 bp, grey), Lifeact-eGFP coding sequence (green, 792 bp), partial sequence from SV40 polyadenylation signal (183 bp, pink), rabbit β-globin 3′ untranslated region (575 bp blue). (I) Change in the MFI in $CD8^+$ T cells from OT-I mice transduced with retrovirus to express Lifeact-EGFP or Lifeact-mCherry, then sorted for ∼30% of the population to exclude high and low expressors such that Lifeact-EGFP expression is comparable to that of day 6 LGO1 cells before re-stimulation with peptide-pulsed cognate or non-cognate EL-4 cells for 20 h to generate activated or resting T cells, respectively. Data points are from 3 (Lifeact.EGFP) or 2 (Lifeact-mCherry) independent experiments performed in triplicate. ns: $P>0.05$ by one-sample *t*-test compared with a hypothetical test value of 0.

(LatA) treatment, activated LGO1 T cells retained their enhanced fluorescence, whereas Phalloidin staining was fully abolished (Fig. S3D). We also employed fluorescence lifetime imaging microscopy (FLIM) to determine whether the gain in Lifeact-EGFP fluorescence could be due to a change in the photo-physical characteristics of the fluorophore. FLIM is suitable for detecting dynamic (collisional, FRET) quenching mechanisms, with shortened fluorescence lifetimes indicative of more efficient quenching. In the case of Lifeact-EGFP, FLIM additionally allows the monitoring of changes in the fluorophore microenvironment as the lifetime of GFP depends on the local refractive index, which is related to intracellular crowding (van Manen et al., 2008). By means of a 2D phasor plot of the raw FLIM data (see Materials and Methods), we did not observe any differences in the fluorescence emission decays of resting or activated LGO1 T cells (Fig. 3C). In addition, LatA-mediated disruption of the actin cytoskeleton did not induce changes in the fluorescence lifetime of Lifeact-EGFP (Fig. 3C). These results indicate that the gain in Lifeact-EGFP fluorescence upon activation is independent of the subcellular distribution of F-actin or binding of the reporter thereto, and is not due to quenching or crowding of the fluorophore itself.

By contrast, the GFP signal corresponded directly to an increase in the amount of Lifeact-EGFP protein, as determined by intracellular staining (Fig. 3D) and western blotting (Fig. S3E) using an anti-GFP antibody. Strikingly, we detected no significant increase in eGFP mRNA levels in activated LGO1 CTLs, which expressed high levels of TNF-α and IFN-γ mRNA (Nicolet et al., 2017) (Fig. 3E), suggesting that the gain in Lifeact-EGFP is regulated post-transcriptionally. Post-transcriptional regulation of Lifeact-EGFP is particularly pronounced in naïve T cells, where the marked increase (18.2±1.84 fold change) (Fig. 1H) in GFP signal upon activation was not accompanied by significant increase in mRNA levels (2.51±1.54 fold change) (Fig. 3E). The increase in GFP signal was unaffected by MG-132, a proteasome inhibitor, but was abrogated by cycloheximide (Fig. S3F), further indicating that the increase in GFP signal is not due to its resistance to degradation but is rather a direct consequence of increased Lifeact-EGFP protein synthesis.

To determine the mechanism of translational regulation, we assessed the proportions of ribosomes engaged in polysomes (Fig. 3F,G) and the relative amounts of translationally active polysome-associated transcripts (Fig. S3G). In resting T cells, about 50% of ribosomes are engaged in polysomes; this fraction was significantly reduced after INK128 treatment (Fig. 3G), an inhibitor of the mammalian target of rapamycin (mTOR) kinase, which is consistent with the known effect of mTOR inhibitors to interfere with the recruitment of ribosomes onto mRNAs, i.e. translation initiation. In activated T cells, a lower proportion of ribosomes was accounted for by polysomes, which might reflect faster elongation (whereby ribosomes run off mRNAs more quickly, leading to a lower steady state proportion in polysomes), or lower rates of initiation, or a combination of both (Fig. 3G). Interestingly, INK128 did not affect the proportion of ribosomes engaged in polysomes in activated T cells, suggesting it has no net effect on translation initiation or elongation (Fig. 3G). The majority of eGFP, IFNγ and β2-microglobulin (β2M) mRNA transcripts are associated with polysomes in both resting and activated T cells (Fig. S3G). INK128 treatment induced a specific redistribution of eGFP and IFNγ, but not β2M, mRNA into smaller polysomes (Fig. S3G), consistent with specific impairment of initiation of translation of the eGFP and IFNγ mRNAs. By contrast, in activated T cells, INK128 treatment induced a shift of all three mRNAs from smaller into larger polysomes (Fig. S3G). Taken together with the observations that Lifeact-EGFP protein levels are higher in activated cells and are markedly decreased by INK128, and the observation that its mRNA is found in larger polysomes upon INK128 treatment, our results suggest that INK128 impairs the rate of translation elongation, thereby reducing the synthesis of Lifeact-EGFP in activated T cells. Given that the other two mRNAs behave similarly, this appears to be

Journal of Cell Science (2020) 133, jcs238014. doi:10.1242/jcs.238014

a general, rather than a transcript-specific, effect. An alternative explanation for the effect of INK128 to promote polysomal association of mRNAs in activated cells would be that it activates translation initiation; however, there is no known mechanism by which inhibition of mTOR signalling can activate initiation (Proud, 2019).

As activation-induced synthesis of GFP is unique to the Lifeact-EGFP reporter mouse, we sought to identify the site(s) of Lifeact-EGFP transgene insertion by whole genome sequencing (see Materials and Methods). Results indicate that the mouse is heterozygous for the transgene; with a single insertion site comprising a single copy of the Lifeact-EGFP transgene identified on chromosome 7, where a 44 kb deletion including the BAG family molecular chaperone regulator 3 (BAG3) gene occurred (Fig. 3H). This is consistent with the lack of homozygous Lifeact-EGFP littermates in our colony, since BAG3 homozygous deletions or mutations are lethal (Homma et al., 2006). When Lifeact-EGFP and Lifeact-mCherry coding sequences lacking the 5′ and 3′ untranslated regions (UTRs) were introduced into OT-I T cells by retroviral transduction, we did not detect increases in GFP or mCherry fluorescence upon activation (Fig. 3I). However, when we amplified and compared genomic sequences between the Lifeact-EGFP and Lifeact-RFP mice, the immediate 5′ and 3′ UTR sequences that flank the transgenes were found to be common (Fig. S3H). This would be expected, since they were cloned into similar vectors prior to oocyte transfer during generation of the transgenic mice (Riedl et al., 2010). This indicates that the UTRs are unlikely to be involved in the Lifeact-GFP-specific gain of fluorescence. Furthermore, chromosome 7-specific primers paired with primers targeted to shared regions of Lifeact-EGFP and Lifeact-RFP confirmed the insertion site of Lifeact-EGFP but failed to generate any amplicons from Lifeact-RFP genomic DNA, indicating that the Lifeact-RFP transgene was not inserted at the same locus.

The Lifeact-EGFP reporter enables identification and tracking of individual T cell activation

Since the gain in GFP fluorescence in LGO1 T cells was reliably detected by flow cytometry and sustained for 48 h, we tested if it was suitable for tracking T cell activation in *in vivo* experiments. To this end, LGO1 CTLs were adoptively transferred into mice engrafted with tumours expressing cognate antigen or non-cognate tumours on contralateral flanks (Fig. 4A). Whereas TCR Vα2 was downregulated in all LGO1 CTLs isolated from cognate antigen-expressing tumours, suggesting they had all been activated upon antigen re-encounter, only a subset had upregulated IFN-γ production, with a corresponding increase in GFP intensity. (Fig. 4B; Fig. S4A). By contrast, CTLs isolated from the spleen and contralateral non-cognate tumours did not downregulate TCR Vα2; neither did they express IFN-γ or display an increase in GFP fluorescence (Fig. 4B; Fig. S4A), indicating that Lifeact-EGFP gain is a sensitive reporter of T cell activation *in vivo*.

We next defined a broadly applicable method to identify T cell activation levels in imaging data. Using simple image analysis and a three-sigma interval statistical method – based on Lifeact-EGFP fluorescence intensity and the thereby derived likelihood of a given cell not belonging to the unactivated population – we defined four states that describe both the certainty and extent of activation: indeterminate, low, medium and high (see Materials and Methods and Fig. 4C). By applying these intensity thresholds to LGO1 cells imaged during a cognate search and kill assay, we detected a drop in the indeterminate subpopulation over time, concomitant with an increase in all three activated subpopulations (Fig. 4D; Movie 3). As expected in a non-cognate context, the majority of LGO1 cells remained in the 'indeterminate' group, where the cells cannot confidently be identified as activated (Fig. 4D; Movie 4). After 12 h in a cognate environment, approximately half of the tracked LGO1 cells were identifiable as highly activated with near certainty, i.e. with only a 0.14% likelihood of not being activated (Fig. 4E). Thus, this intensity-based statistical thresholding method readily identifies activated T cell subpopulations in imaging data.

We next imaged at high magnification LGO1 CTLs migrating in a 3D collagen matrix and undergoing activation in a temporally controlled manner via acute exposure to monomeric pMHC. Upon addition of cognate pMHC to the bathing medium, the CTL population rapidly stopped moving (Fig. S4B) in contrast to the addition of a control pMHC, which did not result in any detectable change in instantaneous speed (Fig. S4B). By tracking individual cells exposed to cognate pMHC, we observed that LGO1 T cells gradually changed from a polarised migratory state with an F-actin-rich leading edge and F-actin-poor uropod to a rounded morphology with a more uniform distribution of F-actin (Fig. 4G; Movie 5), which was not observable in the presence of control pMHC (Fig. S4C). Furthermore, by applying a similar intensity-based statistical thresholding method as above, we could monitor individual T cell progression through stages of activation (Fig. S4D). Following exposure to cognate pMHC, T cells stopped migrating (Fig. 4F) and sequentially progressed through the four delimited states, from indeterminate to highly activated, as they increased in GFP fluorescence intensity (Fig. 4G; Movie 5). On average, LGO1 T cells reached the highly activated state 5.7±1.4 h following stimulation with cognate pMHC (Fig. 4H), consistent with our results obtained via population-wide divergence analysis of LGO1 CTLs in cognate versus non-cognate search and kill assays (Fig. 1C), notwithstanding the different method of activation.

DISCUSSION

Real-time *ex vivo* and intravital imaging approaches are now widely employed to visualise cellular functions and behaviour, complemented by a selection of fluorescent reporters. We show that the widely used Lifeact-EGFP reporter of F-actin dynamics also serves as a real-time indicator of individual $CD4^+$ and $CD8^+$ T cell activation. A marked increase in GFP intensity is reliably detectable by flow cytometry and fluorescence microscopy, both following naïve T cell priming and antigen re-encounter by effector T cells. The Lifeact-EGFP reporter thus enabled us to track distinct search, arrest and killing functions of primary effector T cells in a search-and-kill assay, and to identify T cell activation on a population and individual level. We were also able to monitor the subcellular F-actin dynamics, motility and morphological characteristics of T cells, extending our ability to study rapid subcellular changes that precede, accompany or follow T cell activation. Since the Lifeact-EGFP fluorescence gain is sustained, we could also sort T cells based on activation levels for downstream experiments and track T cell activation in *in vivo* experiments, with future potential to monitor *in situ* activation by intravital imaging.

The gain in Lifeact-EGFP fluorescence correlates with late phase activation and effector cytokine production. Basal GFP expression enables tracking of T cells before they are activated, providing an advantage over reporters that fluoresce only upon cytokine production [including TNF-α (Shebzukhov et al., 2014) and IL-2 (Naramura et al., 1998)] and hence require additional vital dye labelling; or reporters that monitor the translocation of nuclear factor of activated T cells (NFATs) (Lodygin et al., 2013) that require an additional constitutive nuclear label. It will be interesting

Journal of Cell Science (2020) 133, jcs238014. doi:10.1242/jcs.238014

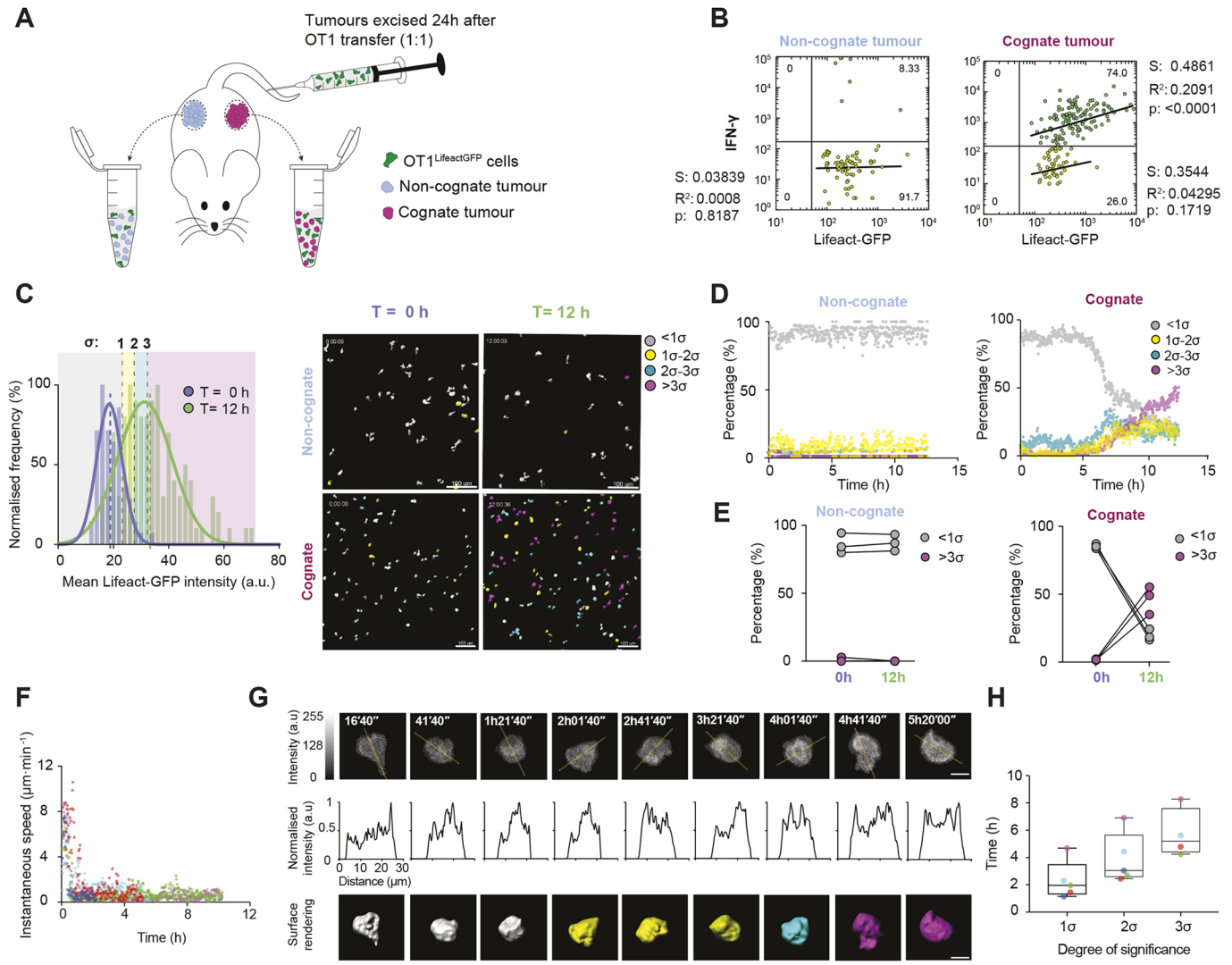

Fig. 4. Identification of different stages of T cell activation using the Lifeact-eGFP reporter mouse. (A) Schematic of RAG1N10 mice bearing cognate and non-cognate EL4 tumours on contralateral flanks. After 24 h of adoptive LGO1 cell transfer, tumours were digested with collagenase IV to release tumour cells and tumour-infiltrating cells for flow cytometry analysis. (B) Correlation analysis of LifeactGFP intensity and the expression of IFN-γ detected by intracellular cytokine staining in tumour-infiltrating LGO1 cells 24 h after adoptive transfer into tumour-bearing mice as described in A. Representative plots from five independent experiments. S, slope; R^2, coefficient of correlation. (C) Distribution of GFP MFI of LGO1 cells co-embedded with cognate EL4 tumour cells (left) at 0 h (purple) or 12 h (green). Black dashed lines: intensity cutoffs at 1, 2 and 3 standard deviations (σ) from the mean at t=0 to delimit LGO1 cell subpopulations per certainty of activation over time. Grey: indeterminate (GFP<$\mu_{t=0}$+1$\sigma_{t=0}$); yellow: low ($\mu_{t=0}$+1$\sigma_{t=0}$≤GFP<$\mu_{t=0}$+2$\sigma_{t=0}$); cyan: medium ($\mu_{t=0}$+2$\sigma_{t=0}$≤GFP<$\mu_{t=0}$+3$\sigma_{t=0}$); magenta: high (GFP≥$\mu_{t=0}$+3$\sigma_{t=0}$) activation confidence level. Purple and green dashed lines: mean GFP fluorescence intensity at t=0 and t=12 h, respectively. Surface-rendered and pseudocoloured LGO1 cells co-embedded with non-cognate or cognate tumour cells at 0 h and 12 h are shown on the right. Surface colour represents the extent and confidence level of activation of LGO1 cells, based on the 3-sigma interval method. Scale bars: 100 µm. (D) Change in the relative frequencies of LGO1 cell subpopulations based on the degree and certainty of T cell activation over time when co-embedded with non-cognate (left) or cognate (right) EL4 tumour cells in 3D collagen matrices. Plots representative of 3 independent experiments. Colours represent the extent and confidence level of activation of LGO1 cells, based on the 3-sigma interval method. (E) Proportion of indeterminate (<1σ; grey) and highly activated LGO1 cells (>3σ; magenta) at 0 h and 12 h in non-cognate (left) or cognate (right) environment as indicated in 3 independent experiments. (F) Instantaneous speeds for the 5 individual (data points) LGO1 cells following acute addition of monomeric cognate pMHC at 0 h. (G) Maximum intensity projections of F-actin localisation (Lifeact-EGFP) in an LGO1 cell embedded in 3D collagen gel following acute addition of dissolved cognate pMHC at 0 h (top). Orange lines indicate region of intensity linescan analysis shown in middle panel. Pseudocoloured surface rendering showing the 3D morphology and the activation level of the LGO1 cell based on our intensity-based statistical thresholding method (bottom; confidence levels by colour as in panel C). Scale bars: 5 µm. (H) Time by which 5 individual LGO1 cells (data points) reach each activation certainty level cutoffs, or degree of significance (σ) after acute addition of cognate pMHC peptide as described in Fig. S4D.

to compare the Lifeact-EGFP sensitivity and specificity with the Nur77^{EGFP} reporter (Au-Yeung et al., 2014), in which GFP is expressed from the immediate early gene *Nr4a1* (Nur77) locus and can rapidly and specifically be induced upon antigen receptor triggering. The Lifeact-EGFP reporter is unsuitable for monitoring proximal and transient TCR signalling, events for which fluorescently-tagged TCR (Friedman et al., 2010; Neve-Oz et al., 2015), Lat (Azar et al., 2010) and Zap-70 (Neve-Oz et al., 2015) FRET-based systems or genetically encoded calcium indicators (GECIs) (Mues et al., 2013; Thestrup et al., 2014) have been employed. The Lifeact-EGFP reporter is likely to prove more valuable in *in vivo* and clinical settings, where sustained signals are more favourable than transient ones for identification and selection of activated cell cohorts or individuals.

The activation-induced gain in Lifeact-EGFP fluorescence is translationally controlled. Polysome analyses in this study showed that global translation, translation discrimination and the mTOR-dependent regulation of translation initiation and elongation phases are distinct in resting and activated T cells, consistent with the increasingly appreciated complexity of translational regulation of immune functions. The Lifeact-EGFP reporter may well prove valuable for investigating other leukocytes and non-immune cell types that employ translational regulation upon activation, maturation or differentiation.

MATERIALS AND METHODS

Isolation and culture of effector T cells from different mouse strains

Lifeact-EGFP mice (Riedl et al., 2010) (a gift from E. Hardeman and R. Wedlich-Söldner) and *mT/mG* (membrane tdTomato) reporter mice (Muzumdar et al., 2007) were crossed to OT-I mice (a gift from E. Deenick) and the resultant Lifeact-EGFP×OT-I (LGO1) and *mT/mG*.OT-I strains bred and housed at Australian BioResources (Moss Vale, NSW, Australia). gBT-1 TCR transgenic mice with TCR specific for H-2K^b/SSIEFARL (Coles et al., 2003) that had been crossed to UBI-GFP mice (expressing GFP under control of the human Ubiquitin C promoter) (Schaefer et al., 2001) (gBT-I.EGFP) were a kind gift from W. R. Heath, and Lifeact-mRFPruby mice (Riedl et al., 2010) were a kind gift from E. Hardeman.

Mouse spleens were dissociated in a 70 µm cell strainer then washed with 10 ml T cell medium (TCM) (TCM: RPMI 1640; 10% heat-inactivated foetal calf serum (HI-FCS); 1 mM sodium pyruvate; 10 mM HEPES; 100 U/ml penicillin; 100 µg/ml streptomycin; 50 µM β-mercaptoethanol (Gibco, Thermo Fisher Scientific, Waltham, MA, USA). Splenocytes were centrifuged at 227 ***g*** for 5 min and resuspended in 1 ml red cell ACK lysis buffer (Gibco, Thermo Fisher Scientific) at 4°C for 1 min. A further 10 ml of TCM was added to the cell suspension and passed through the same strainer before centrifugation, as above. For OT-I strains, 3×10^6 splenocytes were seeded in 10 ml TCM per 25 cm^3 flask (incubated upright) and pulsed with 1 µg/ml SIINFEKL or SSIEFARL peptide (Auspep, Melbourne, VIC, Australia) for OT-I or gBT-I, respectively, for 4 h at 37°C and 5% CO_2, washed and returned to 10 ml warm, fresh TCM for further incubation at 37°C, 5% CO_2. The following day (day 1), cells were washed and resuspended in fresh TCM supplemented with 100 ng/ml mouse IL-2 (R&D Systems, Minneapolis, MN, USA). Cells were then cultured to day 6, expanded based on confluency and replenished with fresh TCM and IL-2 every 1-2 days.

To generate polyclonal effector T cells from non-TCR transgenic Lifeact-EGFP or Lifeact-mRFPruby mice, splenocytes were stimulated for 24 h *in vitro* with 1 µg/ml anti-CD3 (clone: 145-2C11; BioLegend, San Diego, CA, USA), 1 µg/ml anti-CD28 (clone: 37.51; BioLegend) and 100 ng/ml IL-2 in 10 ml of TCM before washing and expansion in TCM and IL-2 until day 6 as above. In some experiments, cells were frozen on day 3 at 3×10^6 cells/ml in 10% dimethyl sulfoxide (DMSO) in heat-inactivated FCS as described (Galeano Niño et al., 2016), and thawed for expansion until day 6 before use.

Real-time 'search-and-kill' assay in 3D collagen gels

Effector CD8$^+$ T cells were cultured to day 6 as described above, whereas EL-4 mouse lymphoma cells (a gift from G. Logan) were maintained in TCM and pulsed overnight with 1 µg/ml SIINFEKL to generate cognate target cells. Un-pulsed EL-4 cells were used as non-cognate controls. EL-4 cells were stained with 1 µM CellTracker Deep Red dye (Thermo Fisher Scientific) as per manufacturer's instructions and allowed to recover for 30 min at 37°C before use. T cells and stained EL-4 cells (cognate or non-cognate) were counted and the following was performed on ice: 1.5×10^5 T cells and 1.5×10^5 EL-4 cells were dispensed into the same 1.5 ml Eppendorf tube and centrifuged at 227 ***g*** for 5 min. The co-pelleted cells were resuspended in 40 µl ice-cold TCM and 10 µl of 10× PBS and 1.14 µl of 1 M NaOH added. Next, 50 µl of ice-cold rat tail collagen type I (Corning, One Riverfront Plaza, NY, USA) was added, quickly mixed and 70 µl of cell-collagen mixture immediately transferred to a single well of a 96-well imaging plate (Greiner Bio-One, Kremsmünster, Austria). The gels were set at 37°C for 10 min prior to addition of 200 µl pre-warmed, Phenol Red-free TCM containing 1 µg/ml propidium iodide (PI) (Thermo Fisher Scientific). Four-dimensional imaging data was collected through a 10× dry objective with a 0.30 numerical aperture on a Leica TCS SP5 confocal microscope (Leica Microsystems, Wetzlar, Germany). Lifeact-EGFP was excited at 488 nm, PI at 561 nm and CellTracker Deep Red Dye at 630 nm using a tuneable white light laser (Leica Microsystems) and emitted light collected within 498-550 nm, 570-620 nm and 640-690 nm, respectively. Data were acquired from the *x*, *y* and *z* planes, with a total *z* depth of 70 µm and a step size of 1.8 µm every 80 s for 12 h.

Image analysis

Imaris 8.4.1 software (Bitplane AG, Zurich, Switzerland) was used to segment cells and PI foci by creating surfaces with a filter of 100 µm^3 to discard cell debris. Cells were tracked using autoregressive motion, applying a threshold of 10 min to filter on track duration. PI foci were tracked using the Brownian motion algorithm. Intensity, morphological and tracking data were then exported and further analysed using GraphPad Prism software (La Jolla, CA, USA). For analysis of killing kinetics in the search-and-kill assay, custom MATLAB (MathWorks, MA, USA) code integrated into Imaris via the XT module (available upon request), retrieves and averages the intensity at the centre of mass of the first two time points of tracked PI foci in both the GFP (T cells) and Deep Red (tumour cells) channels and subtracts the former from the latter:

$$I_{\mathrm{Diff}} = \frac{\sum_{t=0,1} I_{\mathrm{DeepRed}}}{2} - \frac{\sum_{t=0,1} I_{\mathrm{GFP}}}{2}. \quad (1)$$

The resultant intensity difference I_{Diff} was then used to determine the provenance of the PI foci as follows: $I_{\mathrm{Diff}}>10$: PI focus ascribed to a dying tumour cell; $I_{\mathrm{Diff}}<-10$: PI focus ascribed to a dying T cell; $-10\leq I_{\mathrm{Diff}}\leq 10$: PI focus of unknown origin. This last 'unknown' category enables the identification of nuclear debris diffusing into the field of view that ought not to be counted as a 'kill' within the analysed volume.

Re-stimulation of effector cells by cognate tumour cells, antigen-coated beads or antibodies

Effector cell and EL-4 target cell co-cultures were performed in either collagen gels or in suspension (see figure legends). To prepare co-cultures within collagen gels, 1.5×10^5 T cells and 1.5×10^5 EL-4 cells were resuspended in 70 µl ice-cold TCM, 30 µl of which was transferred to a separate tube on ice to establish the input at 0 h. The remaining cell mixture was embedded in collagen as described for the search-and-kill assay above (MatTek, Ashland, MA, USA). To prepare cells for flow cytometry or sorting, cells were released by gel dissociation in 2 ml of warm TCM containing 2% collagenase type IV (Sigma-Aldrich, St Louis, MO, USA) for 25 min at 37°C, washed in 10 ml FACS wash buffer and centrifuged (227 ***g***, 5 min). To prepare co-cultures in suspension, T cells were incubated at a 1:1 ratio with either cognate or non-cognate EL-4 target cells in TCM in 6-well (up to 1×10^6 cells in 3 ml) or 96-well plates (up to 2×10^5 cells in 0.2 ml).

To stimulate effector cells with beads, OT-I cells were co-pelleted with streptavidin beads coated with biotinylated H-2K^b/SIINFEKL peptide (Tetramer Synthesis Service, John Curtin School of Medical Research, Australia National University, ACT, Australia, a gift from K. Gaus). After the indicated incubation times, cells were collected and centrifuged (227 ***g***, 5 min). To stimulate polyclonal effector cells, 5×10^5 cells were incubated for 20 h with streptavidin beads coated with 1 µg/ml biotinylated anti-CD3 (clone: 145-2C11; Thermo Fisher Scientific, Waltham, MA, USA) and 1 µg/ml biotinylated anti-CD28 (clone: 37.51; Thermo Fisher Scientific) monoclonal antibodies or with 1 µg/ml biotinylated IgG2a kappa isotype control (clone: eBR2a; Thermo Fisher Scientific).

Chemical inhibitors

The following inhibitors were used: 10 µM Lck-specific inhibitor, 7-Cyclopentyl-5-(4-phenoxyphenyl)-7H-pyrrolo[2,3-d]pyrimidin-4-ylamine (Calbiochem, Darmstadt, Germany), 10 µM PP2 Src-family kinases inhibitor (Abcam, Cambridge, UK), 10 µM PP3 Src-family kinases

Journal of Cell Science (2020) 133, jcs238014. doi:10.1242/jcs.238014

control (Abcam), 5 µM UO126 (Sigma-Aldrich) Mek1/2 inhibitor, 1 µM latrunculin-A (Abcam), 10 µM cycloheximide (Sigma-Aldrich), 5 µM MG-132 (Sigma-Aldrich), 1 µM INK128 or 0.01% DMSO (Lck inhibitor vehicle). T cells and EL-4 cells were pre-treated for 1 h in the inhibitors, which were also added to the gels or co-cultures for the duration of the experiment.

Surface staining, intracellular protein and cytokine staining for flow cytometry analyses

Where indicated, cells were surface stained with 1.25 µg/ml anti-TCR-β (conjugated with Alexa Fluor 700; clone: H57-597; BioLegend, cat. no. 109223), 1.25 µg/ml^{-1} anti-CD4 (conjugated with fluorescein or phycoerythrin; clone: RM4-4; BioLegend, cat. no. 100511) or 1.25 µg/ml anti-CD8 (conjugated with Pacific Blue; clone: 53-6.7, BioLegend, cat. no. 100728) for 30 min in FACS wash buffer (2% HI-FCS, 2 mM EDTA and 0.02% sodium azide in 1× PBS). Final cell suspensions were prepared in 200 µl cold FACS wash buffer containing 0.5 µg/ml 4′,6-diamidino-2-phenylindole (DAPI) and acquired on the BD Fortessa x20 flow cytometer (BD Biosciences, Franklin Lakes, NJ, USA). Flow cytometry data were analysed with FlowJo software (Treestar Inc., Ashland, OR, USA).

For intracellular staining, cells were first incubated with LIVE/DEAD™ Fixable Aqua Dead Cell Stain (Thermo Fisher Scientific) for 30 min on ice, washed twice, then fixed and permeabilised using the BD Bioscienes Cytofix/Cytoperm™ Plus kit. Permeabilised cells were stained for 45 min with 2.0 µg/ml allophycocyanin-conjugated anti-TNF-α (Clone: MP6-XT22; eBioscience, cat. No. 17-7321-81, San Diego, CA, USA), 2.0 µg/ml phycoerythrin-conjugated anti-IFN-γ (Clone: XMG1.2; BioLegend, cat. no. 505807), rabbit anti-phospho-Zap-70 (Tyr319)/Syk (Tyr352) (1:1000, Cell Signaling Technologies, cat. no. 2717S, Danvers, MA, USA), phospho-p44/42 MAPK (Erk 1/2) (Thr202/Tyr204) (1:200, Cell Signaling Technology, cat. no. 9101S), anti-beta Actin (1:100, Abcam, cat. no. AB8227, Cambridge, UK), 5 U Alexa Fluor 647-conjugated Phalloidin (Invitrogen, cat. no. A22287, Thermo Fisher Scientific) or 1.0 µg/ml Alexa Fluor 647-conjugated anti-GFP (Bioss Antibodies Inc, cat. no. bs-0890R-A647, Woburn, MA, USA) in 1× BD Biosciences Perm/Wash buffer. Where secondary antibody staining is required, cells were centrifuged (227 ***g***, 5 min) and stained for 45 min in goat anti-rabbit IgG conjugated to either 1.0 µg/ml Alexa Fluor 594 (Invitrogen, cat. no. A11037, Thermo Fisher Scientific) or to phycoerythrin (1:100, Invitrogen, cat. no. P-2771MP, cat. no. A11037, Thermo Fisher Scientific). Cells were then centrifuged (227 ***g***, 5 min) and resuspended in 400 µl FACS wash for acquisition on the BD Fortessa x20 flow cytometer (BD Biosciences) and analysis with FlowJo software (Treestar Inc.).

In vitro cytotoxicity assay

EL-4 non-cognate and cognate cells were interchangeably stained with CellTracker Deep Red as described above, mixed in a 1:1 ratio and 1×10^5 of each cell type dispensed into 24W plates in TCM. Effector LGO1 CTLs were pre-treated with 10 µM Lck-specific inhibitor, 5 µM UO126 (Mek1/2 inhibitor) or 0.01% DMSO (vehicle control) for 1 h and 1×10^5 of CTL was added to the mixture of EL-4 cells. TCM containing each inhibitor was further added to achieve final concentrations of 10 µM Lck-specific inhibitor, 5 µM UO126 or 0.01% DMSO in a final volume of 0.5 ml for 12 h. Prior to flow cytometric acquisition, plates were transferred to ice, and 50 µl cold FACS wash buffer containing 0.5 µg/ml DAPI and a reference population of mScarlet-I-expressing EL-4 equivalent to 1×10^4 Spherotech AccuCount Blank Particles (Spherotech, Chicago, IL, USA) was added before acquisition on the BD Fortessa x20 flow cytometer. Absolute cell numbers were calculated and the cytotoxic index calculated as previously described (Galeano Niño et al., 2016) where input and output are numbers at the start and end of the cytotoxic assay, respectively.

Real-time quantitative PCR analyses of gene expression

To prepare cells for RNA extraction, 2×10^6 LGO1 cells were incubated in 3 ml TCM in 6-well plates with equal amounts of either cognate or non-cognate EL-4 cells for 20 h. Cells were then collected and centrifuged (227 ***g***, 5 min) and washed 2× with PBS before being re-suspended in 2 ml cold TCM. A total of 1×10^6 EGFP-expressing LGO1 cells were sorted on the BD FACS Aria III flow sorter (BD Biosciences). Cells were then centrifuged (227 ***g***, 5 min) before RNA isolation using the RNeasy Mini Kit (Qiagen, Hilden, Germany), according to manufacturer's instructions. 1.5 µg of RNA were reverse transcribed to cDNA using the High Capacity cDNA Reverse Transcription Kit (Applied Biosystems, Thermo Fisher Scientific) according to the manufacturer's instructions. Real-time quantitative PCR was carried out using the following primers predesigned and synthesised by Sigma-Aldrich (KiCqStart® SYBR® Green Primers). eGFP-Fwd: 5′-GTAAACGGCCACAAGTTCAGC-3′; eGFP-Rev: 5′-TG-GTGCAGATGAACTTCAGGG-3′; FM1_Rpl13a: 5′-CCTATGACAAG-AAAAAGCGG-3′; RM1_Rpl13a: 5′-CAGGTAAGCAAACTTTCTGG-3′; FM1_B2m: 5′-GTATGCTATCCAGAAAACCC-3′; RM1_B2m: 5′-C-TGAAGGACATATCTGACATC-3′; FM1_Tnf: 5′-CTATGTCTCAGCCT-CTTCTC-3′; RM1_Tnf: 5′-CATTTGGGAACTTCTCATCC-3′; FM1_Ifng: 5-TGAGTATTGCCAAGTTTGAG-3′; RM1_Ifng: 5′-CTTATTGGGAC-AATCTCTTCC-3′; FM1_Actb: 5′-GATGTATGAAGGCTTTGGTC-3′; RM1_Actb: 5′-TGTGCACTTTTATTGGTCTC-3′; FM1_Actg1: 5′-GTA-TCCATGAGACCACTTTC-3′; RM1-Actg1: 5′-CAATGATCTTAATCT-TCATCGTG-3′. 20 ng cDNA was added to each well of a 96-well PCR plate with 1 µM forward and reverse primer for each gene. 40 cycles were performed, with denaturing temperature at 95°C for 15 s, annealing at 55°C for 30 s, and extension at 72°C for 30 s. The amount of amplicon was measured using SYBR Green and detected in a BIO-RAD CFX96 Real time system (Bio-Rad Laboratories, Hercules, CA, USA). The expression of each gene was normalised to the expression of the housekeeping genes β2-microglobulin (β2M) and ribosomal protein L13A (RPL13A).

Quantification of secreted IFN-γ and TNF-α by cytometric bead array

2×10^6 LGO1 cells were cultured overnight together with equal amounts of either cognate or non-cognate EL-4 cells in 6-well plates. LGO1 cells cultured with non-cognate EL-4 cells are considered 'resting', and cells cultured with cognate EL-4 cells are considered 'activated'. Cells were then centrifuged (227 ***g***, 5 min), washed twice with cold PBS and resuspended in 2 ml cold TCM for sorting by flow cytometry. LGO1 cells from non-cognate culture conditions were then used to establish three gates based on Lifeact-EGFP fluorescence intensity in the cognate LGO1 cells: the high gate corresponds to the GFP signal that does not overlap with the intensity of non-cognate LGO1 cells; medium encompasses a portion of the GFP intensity from non-cognate LGO1 cells and low corresponds with the GFP signal that entirely overlaps with the GFP intensity of non-cognate LGO1 cells. Similar gates were drawn in the non-cognate LGO1 cells. 2×10^5 LGO1 cell non-cognate, and 2×10^5 LGO1 cognate cells were then sorted into each of these gates, to give 6 cell populations. After two washes with PBS, sorted cells were cultured into wells of a round-bottomed 96-well plate with 250 µl serum-free TCM. After 4 h, plates were centrifuged (227 ***g***, 5 min) and supernatants collected. Supernatants were then filtered through a 0.22 µm pore filter (Corning, Corning, NY, USA) and IFN-γ and TNF-α cytometric bead array carried out using the LEGENDplex™ Multi-Analyte Flow Assay Kit (BioLegend) as per manufacturer's instructions. 25 µl of each supernatant was mixed with 25 µl of captured beads against TNF-α and IFN-γ for 2 h in a V-bottom plate. After two washes, the samples were incubated with 25 µl of the detection antibody for 1 h followed by the addition of 25 µl of PE-conjugated secondary antibody, both supplied with the kit. Cytokine levels from the supernatants were interpolated from standard curves generated using recombinant proteins from the kit. The data were analysed by FlowJo software.

Western blotting

Cells were lysed in RIPA buffer (25 mM Tris-HCl pH 7.6, 150 mM NaCl, 1% NP-40, 1% sodium deoxycholate, 0.1% SDS) supplemented with protease inhibitors (Halt™ Protease Inhibitor Cocktail (100×) (Thermo Fisher Scientific). Cell debris was pelleted by centrifugation at 12,000 ***g*** for 20 min at 4°C, and the supernatant was used for western blotting. Total protein concentration was determined with Pierce™ BCA Protein Assay Kit (Thermo Fisher Scientific). 30 µg of protein per sample was separated by

Bolt™ 4-12% Bis-Tris gel (Thermo Fisher Scientific) using SeeBlue™ Plus2 Pre-stained Protein Standard (Thermo Fisher Scientific) as a size marker and transferred onto nitrocellulose membranes (Thermo Fisher Scientific). Membranes were probed with primary antibodies against GFP (Abcam, polyclonal), BAG3 (Origene, polyclonal) and Tubulin (Abcam, YL1/2) at 1:1000, 1:1000 and 1:5000 dilutions, respectively. Followed by incubation with secondary antibodies anti-rabbit IgG (Amersham, 1:2000) and goat anti-rat (Thermo Fisher Scientific, 1:10,000). ECL™ Prime Western Blotting Substrate (Merck) was used for detection. Image acquisition of blots was performed on ChemiDoc™ Imaging System (Bio-Rad) and densitometric quantification of bands performed using Image Lab Software (Bio-Rad).

Retroviral transduction of OT-I T cells and EL-4 cells

The following coding sequences were cloned into the murine stem cell virus (MSCV)-based retroviral expression vector and are available upon request: Lifeact-EGFP, Lifeact-mCherry, mTagBFP2-F2A-OVA-Ag85b [which includes the coding sequence for OVA257-264 (SIINFEKL)]. Ecotropic retrovirus was produced by calcium phosphate-mediated transfection of Eco-Pack 2-293 cells (a gift from Y. Wang) using 15 µg of rMSCV-Lifeact-EGFP or 15 µg of rMSCV-Lifeact-EGFP per 4×10^6 cells. Calcium phosphate precipitates were prepared by dropwise addition of 15 µg plasmid DNA (in 0.5 ml of 1 mM Tris, 0.1 mM EDTA, pH 8.0, 0.25 M $CaCl_2$) to 2× HEPES-buffered saline (0.5 ml of 280 mM NaCl, 50 mM HEPES, pH 7.0, 1.5 mM Na_2HPO_4). Precipitates were formed by incubation at room temperature for 20 min and 1 ml of precipitate was added to cells for 16 h. At 48 h after transfection, viral supernatants from 8 dishes were concentrated by high-speed centrifugation (33,403 ***g***, 90 min, 4°C, in a Hitachi R18A fixed angle rotor) and used to transduce 3×10^6 day 1 OT-I T cells activated by SIINFEKL and IL-2 as described above. Transduction was performed in 6-well dishes in the presence of 4 µg/µl Polybrene (Sigma-Aldrich) and centrifuged for 1 h at 2000 ***g*** at 32°C before sorting at 72 h post-transduction (BD FACS Aria III flow sorter, BD Biosciences). Lifeact-EGFP transduced OT-I cells expressing comparable GFP intensities to day 6 LGO1 cells were identified (∼30% of the population) and sorted. As transduction efficiencies were comparable for both Lifeact-EGFP and Lifeact-mCherry, the sort gates were also set on a ∼30% of mCherry-expressing OT-I, excluding high and low-expressors. Sorted cells were recovered for 48 h in TCM before use.

To transduce EL-4 cells, retrovirus pseudotyped with the vesicular stomatitis virus (VSV-G) envelope were produced by polyethylenimine (PEI, molecular weight 4000, PolySciences, cat. no. 24885-2, Warrington, PA, USA) transfection of GP2-293 cells (Clontech, Palo Alto, CA, USA). NaOH-neutralised PEI (1 mg/ml) was complexed with 6.8 µg rMSCV-mTagBFP2-F2A-OVA-Ag85b and 3.2 µg of pMD2.G plasmid (VSVG coding sequence expressed from the CMV promoter) for 30 min at room temperature before addition to 7×10^6 GP2-293 cells. At 72 h after transfection, viral supernatant was used to transduce EL-4 and mTagBFP2-expressing EL-4 were sorted (BD FACS Aria III) 72 h after transduction. Eco-Pack and GP2-293 cells were maintained in DMEM (Gibco) containing 4.5 g/l glucose, 4 mM L-glutamine and 1 mM sodium pyruvate supplemented with 10% heat-inactivated FBS.

Library construction, whole genome sequencing and identification of transgene insertion site

Genomic DNA from a heterozygous Lifeact-EGFP mouse was extracted using the Isolate II Genomic DNA Kit (Bioline, Meridian Life Sciences). The sequencing library was prepared using TruSeq DNA Nano Library Prep (Illumina Inc.), according to the manufacturer's protocols. Paired end sequencing (2×150 bp) was performed on a HiSeq X sequencer (Illumina Inc.), at the KCCG sequencing laboratory, Garvan Institute of Medical Research. We obtained a total yield of 67.47 GB. The pCAG-promoter-Lifeact-EGFP transgene sequence of the Lifeact-EGFP mouse was inferred from the description of the transgene preparation (Niwa et al., 1991; Riedl et al., 2010) without access to the true transgene sequence. The Mouse Dec. 2011 (GRCm38/mm10) assembly reference genome was obtained from the UCSC genome browser data (ftp://hgdownload.soe.ucsc.edu/goldenPath/mm10/bigZips/chromFa.tar.gz) provided by the GRC Mouse Genome (https://www.ncbi.nlm.nih.gov/grc). A reference genome was prepared by combining the inferred pCAG-promoter-Lifeact-EGFP transgene sequence with the mm10 reference genome using STAR Aligner (version 2.5.2b; Dobin et al., 2013) genomeGenerate. Mouse paired end reads were aligned to the mm10/pCAG-promoter-Lifeact-EGFP reference genome using STAR Aligner alignReads. To identify any potential integration sites, chimeric regions joining the pCAG-promoter-Lifeact-EGFP transgene to the mm10 genome segments were identified from the STAR aligner output. Only one integration site was identified. Aligned reads were visualised using the Integrative Genomics Viewer (IGV) (Robinson et al., 2011). A mm10/pCAG-promoter-Lifeact-EGFP reference genome for use with IGV was prepared by concatenating the inferred pCAG-promoter-Lifeact-EGFP reference genome sequence to the mm10 reference genome as an additional contig with indexing using Samtools faidx (version 1.4; Li et al., 2009). Genome alignments in bam format were indexed using bwa (version 0.7.3a-r367; Li and Durbin, 2009). A deletion was suspected at the transgene integration site based on visualisation of reduction of read depth spanning the region between the chimeric regions from both ends of the transgene. The deletion was assessed using CNVNator (version 0.3.3; Abyzov et al., 2011) with root (version 6.14.04; https://root.cern.ch) with analysis of chr7 only. Additional sequences from the pCAG-promoter-Lifeact-EGFP transgene were manually collected from soft clipped reads at the integration site, then manually aligned to generate an additional transgene sequence. As the transgene sequence obtained differed from the inferred sequence, we repeated the above method (genome generate through to IGV visualisation) across 4 additional iterations using the updated transgene sequence each iteration, clarifying and extending additional novel transgene sequence until a near complete transgene sequence was obtained.

Touchdown PCR for amplification of Lifeact-EGFP and Lifeact-mRFPruby transgenes

Genomic DNA was extracted from 3-5 million T cells isolated from the Lifeact-EGFP×OT-1 and Lifeact-mRFPruby mouse using the Isolate II isolation kit (Bioline) and subject to Touchdown PCR using a combination of the following primer pairs (100 ng of primer per 50 µl reaction) with PfU-Ultra polymerase (Agilent Technologies, now Integrated Sciences, NSW, Australia): GFP-Fwd 5′-GTCCTGCTGGAGTTCGTGAC-3′; Ruby-Fwd 5′-GGACTACACCATCGTGGAACA-3′; Rabbit-Rev 5′-CCCATATGTC-CTTCCGAGTG-3′; Ch7-Fwd 5′-TAAGCAAGATCTTAGCTTCAAAC-TCCCAGTCTATGG-3′;Ch7-Rev 5′-TAAGCAGTCGACACTTAGAGT-CACCGTTCAAACACA-3′; Rabbit-Fwd 5′-CACTCGGAAGGACATAT-GGG-3′; CAG-Fwd 5′-TCCGCGTTACATAACTTACGG-3′; CAG-Rev 5′-GGGCGTACTTGGCATATGAT-3′. Additional primers as per Fig. S3H were as follows: A: 5′-ACGGGGTCATTAGTTCATAGCC-3′ and 5′-GG-GCGTACTTGGCATATGAT-3′; B: 5′-ACGGGGTCATTAGTTCATAG-CC-3′ and 5′-AGATGGGGAGAGTGAAGCAGA-3′; C: 5′-TCCGCG-TTACATAACTTACGG-3′ and 5′-GGGCGTACTTGGCATATGAT-3′; D: 5′-TCCGCGTTACATAACTTACGG-3′ and 5′-AGATGGGGAGAGTG-AAGCAGA-3′; E: 5′-TCTGCTTCACTCTCCCCATCT-3′ and 5′-GCGC-TAATTACAGCCCGGA-3′; F: 5′-CGCTGCGTTGCCTTCGC-3′ and 5′-TCGCACGATTACCATAAAAGGCA-3′; G: 5′-CGTGTGTGTGTGCG-TGGG-3′ and 5′-TCGCACGATTACCATAAAAGGCA-3′; H: 5′-TGCC-TTTTATGGTAATCGTGCGA-3′ and 5′-GCTTCCCTCCATCTTGACC-TTAA-3′; I: 5′-CCGAAATCTGGGAGGCGC-3′ and 5′-CAATCTCGA-ACTCGTGTCCGT-3′; J: 5′-GGACTACACCATCGTGGAACA-3′ and 5′-CCCATATGTCCTTCCGAGTG-3′; K: 5′-CACTCGGAAGGACATATG-GG-3′ and 5′-GAAGAGGGACAGCTATGACTGG-3′; L: 5′-CACTCGG-AAGGACATATGGG-3′ and 5′-CAGGTCGAGGGATCTTCATA-3′. After an initial denature step (2 min, 95°C), 10 touchdown PCR cycles [denature (30 s, 95°C), anneal (30 s, reducing at 1°C per cycle from 69°C to 59°C), extension (3 min 19 s, 72°C)] followed by 25 standard cycles [denature (30 s, 95°C), anneal (30 s, 59°C), extension (3 min 19 s, 72°C)] were performed before final extension (5 min, 72°C). Products were separated on 1-2% agarose gels, excised and purified (Wizard SV Gel Clean Up Kit, Promega, Madison, WI) before sequencing using 32 pmol of the amplification primers (Ramaciotti Centre for Genomics, UNSW, Sydney, Australia).

Journal of Cell Science (2020) 133, jcs238014. doi:10.1242/jcs.238014

Activation of OT-I T cells *in vivo*

A total of 1×10^6 EL-4 cells transduced to express mTagBFP2 and OVA-Ag85 bicistronically (cognate EL-4) or non-cognate untransduced EL-4 were separately injected subcutaneously into each flank of 8-week-old Rag-deficient B6.SVJ129-Rag1^{tm1Bal}/Arc mice ('RAG1N10', Australian BioResources, NSW, Australia). The tumours were allowed to grow for 6 days before 1×10^7 LGO1 day 6 effector cells were adoptively transferred to the mice via tail vein injection in 200 µl PBS. Twenty-four hours post T cell transfer, mice were euthanised by CO_2 asphyxiation. The spleens and both tumours were collected and dissociated with 1 mg/ml collagenase IV (Sigma-Aldrich) for 30 min at 37°C (shaking at 800 rpm). The samples were filtered through 70 µm cell strainers to obtain single cell suspensions. Tumours or spleens were resuspended in final volumes of 2 ml or 5 ml FACS wash buffer, respectively. 100 µl of cells from these suspensions were mixed with 100 µl of counting beads equivalent to 2×10^4 beads (Spherotech AccuCount Blank Particles; Chicago, IL, USA) to determine the absolute number of infiltrating cells. Remaining cells were stained with 2.0 µg/ml anti-TCRVα2 (conjugated with APC/Cy7; Clone: B20.1; BioLegend, cat. no. 127818) antibody and LIVE/DEAD™ Fixable Aqua Dead Cell Stain (Invitrogen). Cells were fixed and permeabilised using the BD Cytofix/Cytoperm™ Plus kit for IFN-γ intracellular staining as described above before acquisition on a BD Bioscience Fortessa x20 flow cytometer (BD Biosciences).

Cell culture, treatment and lysis for polysome analyses

LGO1 effector T cells were incubated at a 1:1 ratio with cognate EL-4 target cells in T25 flasks, upright (up to 12×10^6 cells each in 24 ml TCM) or were incubated in TCM only for 20 h, in the presence of INK128 (1 µM) or vehicle. Live cells were enriched by layering over 14 ml of Ficoll-Paque™ PLUS (density 1.077 g/ml; GE Healthcare, Pittsburgh, PA) and centrifugation at 400 ***g*** without brakes at room temperature. Live cells collected from the buffy layer were washed twice in TCM and pelleted at 277 ***g***. An aliquot of cells analysed by DAPI staining and flow cytometry demonstrated efficient removal of EL4 tumour debris (90% purity). Cell pellets were resuspended in polysome lysis buffer [1% (v/v) Triton X-100, 10 mM Tris-HCl (pH 7.5), 10 mM NaCl, 10 mM MgCl, 3.3 mM dithiothreitol (DTT), sodium deocycholate 10 µg/ml and 0.13 Units/µl recombinant RNAsin ribonuclease inhibitor (Promega, Madison, WI)], immediately snap frozen in liquid nitrogen and stored at −80°C until analysis. A549 (human lung carcinoma) cells were cultured in pH 6.7 buffered DMEM (Dulbecco's modified Eagle medium, Sigma-Aldrich, Castle Hill, NSW, Australia) supplemented with 10% (v/v) fetal bovine serum (FBS) and 100 U/ml penicillin and 0.1 mg/ml streptomycin, and maintained at 37°C for 16 h in humidified air with 5% (v/v) CO_2. Primary mouse cortical neurons or A549 cells were collected by trypsinization, washed twice with PBS (phosphate-buffered saline, Thermo Fisher Scientific, North Ryde, NSW, Australia) and lysed in ice-cold lysis buffer [1% (v/v) Triton X-100, 20 mM Tris-HCl (pH 7.5), 150 mM NaCl, 1 mM EDTA, 1 mM EGTA, 2.5 mM $NaH_2P_2O_7$, 1 mM β-glycerophosphate, 1 mM dithiothreitol (DTT), 1 mM Na_3VO_4 and protease inhibitor cocktail (1×)]. Lysates were centrifuged at 16,000 ***g*** and 4°C for 10 min and total protein concentrations in the supernatants quantified by Bradford assay. Where indicated, insoluble pellets were dissolved in 1× Laemmli sample buffer [62.5 µM Tris-HCl pH 6.8, 1% (w/v) SDS, 10% (v/v) glycerol, 10 µM DTT and 5 µg/ml Bromophenol Blue].

Polysome analysis was performed as previously described (Xie et al., 2019b). For RNA extraction, 1% (w/v) SDS and 0.15 mg/ml proteinase K were added to each fractions, 1:3 (v/v) phenol:chloroform pH 4.5 was then added to the samples to extract RNA, RNA were precipitated from the aqueous phase by the addition of 70% (v/v) isopropanol. RNA pellets were washed once with 80% (v/v) ethanol, before dissolving in RNase/DNase-free water for further analysis.

Total RNA was extracted using TRIzol (Life Technologies). cDNA was produced using the ImProm-II reverse transcription (RT) system (Promega) with oligo(dT)15. For qPCR analysis of sucrose gradient fractions, 1.2 kb kanamycin RNA provided by the RT kit was used as an internal control. qPCR was performed using the primers indicated in the RT-qPCR section above. Samples were analysed with SYBR green dye mix (Life Technologies) on an ABI Step One Plus qPCR instrument (Applied Biosystems, Cheshire, UK). For total RNA analysis, *B2M* was used as the normalisation control. The comparative threshold cycle (C_T) method was applied to quantify mRNAs present in each sample.

Statistical analyses were performed using a one-way or two-way ANOVA with an unpaired Student's *t*-test with the means of three to four biological replicates as specified. Data are presented as means±s.d., GraphPad Prism software was used to calculate *P*-values. *$0.01\leq P<0.05$; **$0.001\leq P<0.01$; ***$P<0.001$.

T cell activation by soluble pMHC during 4D imaging

For high-resolution tiled 40× (dry objective with 0.75 NA, Leica Microsystems, Wetzlar, Germany) time-lapse imaging, LGO1 cells were embedded in collagen gels as described above, but in the absence of EL-4 cells. Gels were imaged for 1 h before the addition of 1 µg/ml biotinylated H-2K^b/SIINFEKL monomers (Tetramer Synthesis Service, John Curtin School of Medical Research, Australia National University, ACT, Australia, a gift from K. Gaus) in 50 µl to the bathing medium, after which gels were imaged for a further 10 h. As a control, H2K^b/RGYVYQGL biotinylated monomers (Tetramer Synthesis Service, John Curtin School of Medical Research, Australia National University, ACT, Australia, a gift from K. Gaus) were added to the medium. Data was analysed using the Imaris software as described above.

Statistical identification of activated T cell subpopulations in live-cell imaging data

We examined cell fluorescence intensity values from imaging data at $t=0$ h, when cells are still considered to be unactivated. As the fluorescence intensity values display a Gaussian distribution (D'Agostino & Pearson omnibus K2 test; $P=0.1885$ with a null hypothesis that the data are sampled from a Gaussian distribution) 99.7% (∼100%) of values will fall within 3 standard deviations (σ) of the mean (μ). Therefore, we defined a fluorescence intensity threshold of $\mu_{t=0}+3\sigma_{t=0}$, where at any given time point, cells displaying a fluorescence intensity above this can be considered with near-certainty as not belonging to the unactivated population, i.e. are certainly activated, and were designated as belonging to the 'high' level of activation cohort (magenta). We then applied this sigma-based selection criteria to reflect three further levels of activation; cells exhibiting a fluorescence intensity (GFP) of $GFP<\mu_{t=0}+1\sigma_{t=0}$, considered 'indeterminate' (grey), cells where $\mu_{t=0}+1\sigma_{t=0}\leq GFP<\mu_{t=0}+2\sigma_{t=0}$ were assigned a 'low' level of activation (yellow), and cells exhibiting a fluorescence intensity of $\mu_{t=0}+2\sigma_{t=0}\leq GFP<\mu_{t=0}+3\sigma_{t=0}$ were assigned a 'medium' level of activation (cyan). This method is easily implementable for the determination of activation state and certainty where an unactivated reference population is available (either at $t=0$ in a temporal experiment or as a separate condition).

Determination of characteristic time of divergence of Lifeact-EGFP intensity between cognate and control populations

All analysis steps in this section were performed with the help of custom MATLAB (MathWorks, MA, USA) routines, available upon request.

Normalisation and photo-bleaching correction

Time-series of fluorescence intensity distributions of Lifeact-EGFP fluorescence signals (3 independent series for cognate environment, 3 independent series for non-cognate environment) were normalised to a median of 1 at $t=0$ in order to account for differences in laser powers and systematic variations. Non-cognate condition time-series were pooled, and a mono-exponential decay function [$f(t)=A\cdot e^{\tau\cdot t}$] was fitted to the median of the pooled data. Cognate and pooled non-cognate time-series were divided by the obtained exponential decay function to correct for photo-bleaching. Only normalised and bleach-corrected data sets were used for further analysis.

Divergence analysis

To determine the time of divergence, the non-parametric right-tailed Wilcoxon rank sum test was used to compare the cognate and pooled non-

cognate intensity distributions at each time point. Briefly, the null hypothesis that Lifeact-EGFP fluorescence from non-cognate and cognate intensity distributions are samples from the same continuous distribution is tested against the alternative hypothesis that intensity values of the cognate distribution tend to be larger than the ones of the non-cognate distribution. Three different test significance levels were considered (0.1587, 0.0227, 0.0014 corresponding to a probability of finding values above the mean plus 1, 2 or 3 standard deviations in a normal distribution), stating the probability that the null-hypothesis is falsely rejected. The time of divergence was determined as the first time-point after which all subsequent *P*-values were $P<0.0014$. It should be noted that the maximal temporal difference between matching cognate and non-cognate pairs was 39.6 s, which was considered negligible taking the relevant time-scale (12 h) of the experiment into account.

Determination of characteristic time of activation after addition of cognate pMHC-I

All analysis steps in this section were performed with the help of custom MATLAB (MathWorks, MA, USA) routines, available upon request.

Photo-bleaching correction

Time-series of fluorescence intensity distributions of Lifeact-EGFP signals before ('PRE', 0-52 min) and after ('POST', 52 min signal ending) the addition of cognate H-2K^b/SIINFEKL were determined. 'PRE' single-cell intensity traces were re-aligned to start at t=0 and a mono-exponential decay model function [$f(t)=A \cdot e^{\tau t}$] was fitted to the re-aligned data set. Re-aligned 'PRE' distribution and 'POST' intensity traces of five individual cells were divided by the obtained decay to correct for photo-bleaching. Only bleach-corrected data sets were used for further analysis.

Time of activation

'PRE' fluorescence intensities were pooled and a non-parametric estimation of the underlying probability distribution function (pdf) was obtained by fitting a kernel distribution with a normal kernel smoothing function to the data set. By minimising $f(x_{\mathrm{lim}}) = \left|\int_{x_{\mathrm{lim}}}^{\infty} \mathrm{pdf}(x)\mathrm{d}x - \alpha\right|$ with respect to x_{lim}, intensity thresholds $x_{\mathrm{lim}_{1,2,3}}$ corresponding to specific error probability levels α (i.e. α_1=15.87%, α_2=2.27%, α_3=0.14%) were determined. In other words, the probability to find an intensity value of the 'PRE' intensity distribution greater than $x_{\mathrm{lim}_{1,2,3}}$ equals 15.87%, 2.27%, 0.14%, respectively. By determining the time points corresponding to $x_{\mathrm{lim}_{1,2,3}}$, three activation times with increasing significance were obtained for each 'POST' intensity trace (Fig. 4F; Fig. S4E).

Acquisition of FLIM data

2×10^6 LGO1 cells were incubated for 20 h with equal numbers of either cognate or non-cognate EL-4 cells. Subsequently, half of each population remained untreated (cognate and non-cognate) whereas the other half was treated with LatA for 30 min [cognate (LatA), non-cognate (LatA)]. Prior to imaging, cells were transferred to untreated glass-bottom dishes (Mattek). FLIM data was acquired with a Picoquant Microtime200 setup (Picoquant, Berlin, Germany), using a 60× UPlanSApo NA 1.2 water immersion objective (Olympus, Tokyo, Japan) and a laser pulse frequency of 20 MHz at a wavelength of 470 nm. For each of the four conditions, three different fields of view were imaged.

Analysis of FLIM data

All analysis steps in this section were performed with a custom MATLAB (MathWorks, MA, USA) routine, implementing the phasor plot approach (Digman et al., 2008). Briefly, for each pixel the real (G) and imaginary (S) components of the Fourier transform of the fluorescence emission decay (I) are calculated:

$$G(\omega) = \frac{\int_0^{\infty} I(t)\cos(\omega t)dt}{\int_0^{\infty} I(t)dt} \quad S(\omega) = \frac{\int_0^{\infty} I(t)\sin(\omega t)dt}{\int_0^{\infty} I(t)dt}, \tag{2}$$

with ω depicting the laser pulse angular frequency. At the same time, G and S are equal to:

$$G(\omega) = \sum_{i=1}^{N} \frac{f_i}{1+\omega^2\tau_i} \quad S(\omega) = \sum_{i=1}^{N} \frac{f_i\omega\tau_i}{1+\omega^2\tau_i}\ , \tag{3}$$

with f_i being the relative fraction that the ith species with fluorescence lifetime τ_i contributes to the overall fluorescence intensity. For a single lifetime, the relationship between G and S can be written as a semi-circle equation:

$$(G(\omega)-0.5)^2 + S(\omega)^2 = 0.25, \tag{4}$$

meaning that G-S-pair distributions of samples with a single fluorescence lifetime should be centred on that semicircle. To find the correct scale for the plotted phasor points, the coordinates of the phasor plot were calibrated with Atto488-NHS (ATTO-TEC GmbH, Siegen, Germany) dissolved in water, which has a stable lifetime of 4.2 ns. For three different fields of view in each condition, G-S-pair density distributions were plotted as isocontours, with outer lines corresponding to 15% of the maximum G-S-pair density. As all distributions were approximately centred on the semi-circle, for all data sets the lifetime per pixel was calculated as:

$$\tau = \frac{1}{\omega}\left(\frac{S(\omega)}{G(\omega)}\right). \tag{5}$$

Statistical analysis

Statistical parameters are reported in the figures and legends. Mann–Whitney *U*-tests were used to compare medians between two groups and Kruskal–Wallis test to compare medians between more than two groups followed by Dunn's multiple comparison tests. One-sample *t*-tests were used to compare the mean of the $\log_{10}$ fold change to a hypothetical mean of 0 (no difference between the groups). Statistical analyses were performed using Prism 7.0 (GraphPad Software, La Jolla, CA, USA).

Animal experimentation

Animal breeding and experimentation was conducted in accordance with New South Wales state and Australian federal laws and animal ethics protocols overseen and approved by the University of New South Wales Animal Care and Ethics Committee.

Acknowledgements

The authors thank Sandra Cooper for helpful discussions, Mark Read for technical advice and the BioMedical Imaging Facility and Biological Resources Imaging Laboratory of UNSW for assistance with imaging and flow cytometry, respectively. M.B. acknowledges Bitplane AG for an Imaris Developer licence.

Competing interests

The authors declare no competing or financial interests.

Author contributions

Conceptualization: J.L.G.N., M.B.; Methodology: J.L.G.N., S.S.T., J.L.E.T., D.K., M.B.; Validation: S.S.T., J.M.; Formal analysis: J.L.G.N., S.S.T., J.L.E.T., J.X., M.A.G., D.K., J.M., A.P.D., S.K., C.G.P., M.B.; Investigation: J.L.G.N., S.S.T., J.X., M.A.G., J.M., F.C., C.G.P., M.B.; Resources: M.B.; Writing - original draft: J.L.G.N., S.S.T., M.B.; Writing - review & editing: S.S.T., M.B.; Visualization: J.L.G.N., J.L.E.T., D.K., M.B.; Supervision: S.S.T., S.K., C.G.P., M.B.; Project administration: M.B.; Funding acquisition: M.B.

Funding

This work was supported by funding via European Molecular Biology Laboratory (EMBL) Australia to M.B., and South Australian Health and Medical Research Institute to C.G.P.

Data availability

The whole genome sequence of the Lifeact-EGFP mouse is available via the EMBL-EBI European Nucleotide Archive (ENA) under accession number PRJEB33979.

Supplementary information

Supplementary information available online at
http://jcs.biologists.org/lookup/doi/10.1242/jcs.238014.supplemental

Peer review history
The peer review history is available online at https://jcs.biologists.org/lookup/doi/10.1242/jcs.238014.reviewer-comments.pdf.

References

Abyzov, A., Urban, A. E., Snyder, M. and Gerstein, M. (2011). CNVnator: an approach to discover, genotype, and characterize typical and atypical CNVs from family and population genome sequencing. *Genome Res.* **21**, 974-984. doi:10.1101/gr.114876.110

Araki, K., Morita, M., Bederman, A. G., Konieczny, B. T., Kissick, H. T., Sonenberg, N. and Ahmed, R. (2017). Translation is actively regulated during the differentiation of CD8$^+$ effector T cells. *Nat. Immunol.* **18**, 1046-1057. doi:10.1038/ni.3795

Au-Yeung, B. B., Zikherman, J., Mueller, J. L., Ashouri, J. F., Matloubian, M., Cheng, D. A., Chen, Y., Shokat, K. M. and Weiss, A. (2014). A sharp T-cell antigen receptor signaling threshold for T-cell proliferation. *Proc. Natl. Acad. Sci. USA* **111**, E3679-E3688. doi:10.1073/pnas.1413726111

Azar, G. A., Lemaître, F., Robey, E. A. and Bousso, P. (2010). Subcellular dynamics of T cell immunological synapses and kinapses in lymph nodes. *Proc. Natl. Acad. Sci. USA* **107**, 3675-3680. doi:10.1073/pnas.0905901107

Billadeau, D. D., Nolz, J. C. and Gomez, T. S. (2007). Regulation of T-cell activation by the cytoskeleton. *Nat. Rev. Immunol.* **7**, 131-143. doi:10.1038/nri2021

Bjur, E., Larsson, O., Yurchenko, E., Zheng, L., Gandin, V., Topisirovic, I., Li, S., Wagner, C. R., Sonenberg, N. and Piccirillo, C. A. (2013). Distinct translational control in CD4+ T cell subsets. *PLoS Genet.* **9**, e1003494. doi:10.1371/journal.pgen.1003494

Brown, M. C., Holl, E. K., Boczkowski, D., Dobrikova, E., Mosaheb, M., Chandramohan, V., Bigner, D. D., Gromeier, M. and Nair, S. K. (2017). Cancer immunotherapy with recombinant poliovirus induces IFN-dominant activation of dendritic cells and tumor antigen-specific CTLs. *Sci. Transl. Med.* **9**, eaan4220. doi:10.1126/scitranslmed.aan4220

Chakraborty, A. K. and Weiss, A. (2014). Insights into the initiation of TCR signaling. *Nat. Immunol.* **15**, 798-807. doi:10.1038/ni.2940

Coles, R. M., Jones, C. M., Brooks, A. G., Cameron, P. U., Heath, W. R. and Carbone, F. R. (2003). Virus infection expands a biased subset of T cells that bind tetrameric class I peptide complexes. *Eur. J. Immunol.* **33**, 1557-1567. doi:10.1002/eji.200323715

Digman, M. A., Caiolfa, V. R., Zamai, M. and Gratton, E. (2008). The phasor approach to fluorescence lifetime imaging analysis. *Biophys. J.* **94**, L14-L16. doi:10.1529/biophysj.107.120154

Dobin, A., Davis, C. A., Schlesinger, F., Drenkow, J., Zaleski, C., Jha, S., Batut, P., Chaisson, M. and Gingeras, T. R. (2013). STAR: ultrafast universal RNA-seq aligner. *Bioinformatics* **29**, 15-21. doi:10.1093/bioinformatics/bts635

Favata, M. F., Horiuchi, K. Y., Manos, E. J., Daulerio, A. J., Stradley, D. A., Feeser, W. S., Van Dyk, D. E., Pitts, W. J., Earl, R. A., Hobbs, F. et al. (1998). Identification of a novel inhibitor of mitogen-activated protein kinase kinase. *J. Biol. Chem.* **273**, 18623-18632. doi:10.1074/jbc.273.29.18623

Fehniger, T. A., Cai, S. F., Cao, X., Bredemeyer, A. J., Presti, R. M., French, A. R. and Ley, T. J. (2007). Acquisition of murine NK cell cytotoxicity requires the translation of a pre-existing pool of granzyme B and perforin mRNAs. *Immunity* **26**, 798-811. doi:10.1016/j.immuni.2007.04.010

Friedman, R. S., Beemiller, P., Sorensen, C. M., Jacobelli, J. and Krummel, M. F. (2010). Real-time analysis of T cell receptors in naive cells in vitro and in vivo reveals flexibility in synapse and signaling dynamics. *J. Exp. Med.* **207**, 2733-2749. doi:10.1084/jem.20091201

Galeano Niño, J. L., Kwan, R. Y. Q., Weninger, W. and Biro, M. (2016). Antigen-specific T cells fully conserve antitumour function following cryopreservation. *Immunol. Cell Biol.* **94**, 411-418. doi:10.1038/icb.2015.105

Gerlach, C., Van Heijst, J. W. J., Swart, E., Sie, D., Armstrong, N., Kerkhoven, R. M., Zehn, D., Bevan, M. J., Schepers, K. and Schumacher, T. N. M. (2010). One naive T cell, multiple fates in CD8$^+$ T cell differentiation. *J. Exp. Med.* **207**, 1235-1246. doi:10.1084/jem.20091175

Gorentla, B. K. and Zhong, X. P. (2012). T cell receptor signal transduction in T lymphocytes. *J. Clin. Cell Immunol.* **2012**, 5.

Hanke, J. H., Gardner, J. P., Dow, R. L., Changelian, P. S., Brissette, W. H., Weringer, E. J., Pollok, B. A. and Connelly, P. A. (1996). Discovery of a novel, potent, and Src family-selective tyrosine kinase inhibitor. Study of Lck- and FynT-dependent T cell activation. *J. Biol. Chem.* **271**, 695-701. doi:10.1074/jbc.271.2.695

Hogquist, K. A., Jameson, S. C., Heath, W. R., Howard, J. L., Bevan, M. J. and Carbone, F. R. (1994). T cell receptor antagonist peptides induce positive selection. *Cell* **76**, 17-27. doi:10.1016/0092-8674(94)90169-4

Homma, S., Iwasaki, M., Shelton, G. D., Engvall, E., Reed, J. C. and Takayama, S. (2006). BAG3 deficiency results in fulminant myopathy and early lethality. *Am. J. Pathol.* **169**, 761-773. doi:10.2353/ajpath.2006.060250

Jenkins, M. R., Rudd-Schmidt, J. A., Lopez, J. A., Ramsbottom, K. M., Mannering, S. I., Andrews, D. M., Voskoboinik, I. and Trapani, J. A. (2015). Failed CTL/NK cell killing and cytokine hypersecretion are directly linked through prolonged synapse time. *J. Exp. Med.* **212**, 307-317. doi:10.1084/jem.20140964

Kim, K., Wang, L. and Hwang, I. (2009). A novel flow cytometric high throughput assay for a systematic study on molecular mechanisms underlying T cell receptor-mediated integrin activation. *PLoS ONE* **4**, e6044. doi:10.1371/journal.pone.0006044

Koike, T., Yamagishi, H., Hatanaka, Y., Fukushima, A., Chang, J.-W., Xia, Y., Fields, M., Chandler, P. and Iwashima, M. (2003). A novel ERK-dependent signaling process that regulates interleukin-2 expression in a late phase of T cell activation. *J. Biol. Chem.* **278**, 15685-15692. doi:10.1074/jbc.M210829200

Kumari, S., Curado, S., Mayya, V. and Dustin, M. L. (2014). T cell antigen receptor activation and actin cytoskeleton remodeling. *Biochim. Biophys. Acta* **1838**, 546-556. doi:10.1016/j.bbamem.2013.05.004

Li, H. and Durbin, R. (2009). Fast and accurate short read alignment with Burrows-Wheeler transform. *Bioinformatics* **25**, 1754-1760. doi:10.1093/bioinformatics/btp324

Li, H., Handsaker, B., Wysoker, A., Fennell, T., Ruan, J., Homer, N., Marth, G., Abecasis, G., Durbin, R. and **1000 Genome Project Data Processing Subgroup**. (2009). The Sequence Alignment/Map format and SAMtools. *Bioinformatics* **25**, 2078-2079. doi:10.1093/bioinformatics/btp352

Lodygin, D., Odoardi, F., Schläger, C., Körner, H., Kitz, A., Nosov, M., Van Den Brandt, J., Reichardt, H. M., Haberl, M. and Flügel, A. (2013). A combination of fluorescent NFAT and H2B sensors uncovers dynamics of T cell activation in real time during CNS autoimmunity. *Nat. Med.* **19**, 784-790. doi:10.1038/nm.3182

Love, P. E. and Hayes, S. M. (2010). ITAM-mediated signaling by the T-cell antigen receptor. *Cold Spring Harb. Perspect. Biol.* **2**, a002485. doi:10.1101/cshperspect.a002485

Malik, N. M., Gilroy, D. W. and Kabouridis, P. S. (2009). Regulation of growth and survival of activated T cells by cell-transducing inhibitors of Ras. *FEBS Lett.* **583**, 61-69. doi:10.1016/j.febslet.2008.11.042

Mues, M., Bartholomäus, I., Thestrup, T., Griesbeck, O., Wekerle, H., Kawakami, N. and Krishnamoorthy, G. (2013). Real-time in vivo analysis of T cell activation in the central nervous system using a genetically encoded calcium indicator. *Nat. Med.* **19**, 778-783. doi:10.1038/nm.3180

Mullins, R. D. and Hansen, S. D. (2013). In vitro studies of actin filament and network dynamics. *Curr. Opin. Cell Biol.* **25**, 6-13. doi:10.1016/j.ceb.2012.11.007

Muzumdar, M. D., Tasic, B., Miyamichi, K., Li, L. and Luo, L. (2007). A global double-fluorescent Cre reporter mouse. *Genesis* **45**, 593-605. doi:10.1002/dvg.20335

Naramura, M., Hu, R.-J. and Gu, H. (1998). Mice with a fluorescent marker for interleukin 2 gene activation. *Immunity* **9**, 209-216. doi:10.1016/S1074-7613(00)80603-2

Neve-Oz, Y., Razvag, Y., Sajman, J. and Sherman, E. (2015). Mechanisms of localized activation of the T cell antigen receptor inside clusters. *Biochim. Biophys. Acta* **1853**, 810-821. doi:10.1016/j.bbamcr.2014.09.025

Nicolet, B. P., Guislain, A. and Wolkers, M. C. (2017). Combined single-cell measurement of cytokine mRNA and protein identifies T cells with persistent effector function. *J. Immunol.* **198**, 962-970. doi:10.4049/jimmunol.1601531

Niwa, H., Yamamura, K. and Miyazaki, J. (1991). Efficient selection for high-expression transfectants with a novel eukaryotic vector. *Gene* **108**, 193-199. doi:10.1016/0378-1119(91)90434-D

Piccirillo, C. A., Bjur, E., Topisirovic, I., Sonenberg, N. and Larsson, O. (2014). Translational control of immune responses: from transcripts to translatomes. *Nat. Immunol.* **15**, 503-511. doi:10.1038/ni.2891

Pollizzi, K. N., Waickman, A. T., Patel, C. H., Sun, I. H. and Powell, J. D. (2015). Cellular size as a means of tracking mTOR activity and cell fate of CD4+ T cells upon antigen recognition. *PLoS ONE* **10**, e0121710. doi:10.1371/journal.pone.0121710

Proud, C. G. (2019). Phosphorylation and signal transduction pathways in translational control. *Cold Spring Harb. Perspect. Biol.* **11**, a033050. doi:10.1101/cshperspect.a033050

Riedl, J., Crevenna, A. H., Kessenbrock, K., Yu, J. H., Neukirchen, D., Bista, M., Bradke, F., Jenne, D., Holak, T. A., Werb, Z. et al. (2008). Lifeact: a versatile marker to visualize F-actin. *Nat. Methods* **5**, 605-607. doi:10.1038/nmeth.1220

Riedl, J., Flynn, K. C., Raducanu, A., Gärtner, F., Beck, G., Bösl, M., Bradke, F., Massberg, S., Aszodi, A., Sixt, M. et al. (2010). Lifeact mice for studying F-actin dynamics. *Nat. Methods* **7**, 168-169. doi:10.1038/nmeth0310-168

Ritter, A. T., Asano, Y., Stinchcombe, J. C., Dieckmann, N. M. G., Chen, B.-C., Gawden-Bone, C., Van Engelenburg, S., Legant, W., Gao, L., Davidson, M. W. et al. (2015). Actin depletion initiates events leading to granule secretion at the immunological synapse. *Immunity* **42**, 864-876. doi:10.1016/j.immuni.2015.04.013

Robinson, J. T., Thorvaldsdóttir, H., Winckler, W., Guttman, M., Lander, E. S., Getz, G. and Mesirov, J. P. (2011). Integrative genomics viewer. *Nat. Biotechnol.* **29**, 24-26. doi:10.1038/nbt.1754

Schaefer, B. C., Schaefer, M. L., Kappler, J. W., Marrack, P. and Kedl, R. M. (2001). Observation of antigen-dependent CD8+ T-cell/ dendritic cell interactions in vivo. *Cell. Immunol.* **214**, 110-122. doi:10.1006/cimm.2001.1895

Schott, J., Reitter, S., Philipp, J., Haneke, K., Schafer, H. and Stoecklin, G. (2014). Translational regulation of specific mRNAs controls feedback inhibition and survival during macrophage activation. *PLoS Genet.* **10**, e1004368. doi:10.1371/journal.pgen.1004368

Seo, H.-H., Kim, S. W., Lee, C. Y., Lim, K. H., Lee, J., Lim, S., Lee, S. and Hwang, K.-C. (2017). 7-cyclopentyl-5-(4-phenoxyphenyl)-7H-pyrrolo[2,3-d] pyrimidin-4-ylamine inhibits the proliferation and migration of vascular smooth muscle cells by suppressing ERK and Akt pathways. *Eur. J. Pharmacol.* **798**, 35-42. doi:10.1016/j.ejphar.2017.02.004

Shebzukhov, Y. V., Kuchmiy, A. A., Kruglov, A. A., Zipp, F., Siffrin, V. and Nedospasov, S. A. (2014). Experimental applications of TNF- reporter mice with far-red fluorescent label. *Methods Mol. Biol.* **1155**, 151-162. doi:10.1007/978-1-4939-0669-7_13

Tan, T. C. J., Knight, J., Sbarrato, T., Dudek, K., Willis, A. E. and Zamoyska, R. (2017). Suboptimal T-cell receptor signaling compromises protein translation, ribosome biogenesis, and proliferation of mouse CD8 T cells. *Proc. Natl. Acad. Sci. USA* **114**, E6117-E6126. doi:10.1073/pnas.1700939114

Thestrup, T., Litzlbauer, J., Bartholomäus, I., Mues, M., Russo, L., Dana, H., Kovalchuk, Y., Liang, Y., Kalamakis, G., Laukat, Y. et al. (2014). Optimized ratiometric calcium sensors for functional in vivo imaging of neurons and T lymphocytes. *Nat. Methods* **11**, 175-182. doi:10.1038/nmeth.2773

Van Manen, H.-J., Verkuijlen, P., Wittendorp, P., Subramaniam, V., Van Den Berg, T. K., Roos, D. and Otto, C. (2008). Refractive index sensing of green fluorescent proteins in living cells using fluorescence lifetime imaging microscopy. *Biophys. J.* **94**, L67-L69. doi:10.1529/biophysj.107.127837

Varma, R., Campi, G., Yokosuka, T., Saito, T. and Dustin, M. L. (2006). T cell receptor-proximal signals are sustained in peripheral microclusters and terminated in the central supramolecular activation cluster. *Immunity* **25**, 117-127. doi:10.1016/j.immuni.2006.04.010

Vicente-Manzanares, M. and Sánchez-Madrid, F. (2004). Role of the cytoskeleton during leukocyte responses. *Nat. Rev. Immunol.* **4**, 110-122. doi:10.1038/nri1268

Wang, H., Kadlecek, T. A., Au-Yeung, B. B., Goodfellow, H. E. S., Hsu, L. Y., Freedman, T. S. and Weiss, A. (2010). ZAP-70: an essential kinase in T-cell signaling. *Cold Spring Harb. Perspect. Biol.* **2**, a002279. doi:10.1101/cshperspect.a002279

Weninger, W., Biro, M. and Jain, R. (2014). Leukocyte migration in the interstitial space of non-lymphoid organs. *Nat. Rev. Immunol.* **14**, 232-246. doi:10.1038/nri3641

Xie, J., De Souza Alves, V., Von Der Haar, T., O'keefe, L., Lenchine, R. V., Jensen, K. B., Liu, R., Coldwell, M. J., Wang, X. and Proud, C. G. (2019a). Regulation of the elongation phase of protein synthesis enhances translation accuracy and modulates lifespan. *Curr. Biol.* **29**, 737-749.e5. doi:10.1016/j.cub.2019.01.029

Xie, J., Van Damme, P., Fang, D. and Proud, C. G. (2019b). Ablation of elongation factor 2 kinase enhances heat-shock protein 90 chaperone expression and protects cells under proteotoxic stress. *J. Biol. Chem.* **294**, 7169-7176. doi:10.1074/jbc.AC119.008036

Yeh, J.-H., Sidhu, S. S. and Chan, A. C. (2008). Regulation of a late phase of T cell polarity and effector functions by Crtam. *Cell* **132**, 846-859. doi:10.1016/j.cell.2008.01.013

Zhao, F., Cannons, J. L., Dutta, M., Griffiths, G. M. and Schwartzberg, P. L. (2012). Positive and negative signaling through SLAM receptors regulate synapse organization and thresholds of cytolysis. *Immunity* **36**, 1003-1016. doi:10.1016/j.immuni.2012.05.017

The Lifeact-EGFP Mouse is a Translationally Controlled Fluorescent Reporter of T Cell Activation

Jorge Luis Galeano Niño[†], Szun S. Tay[†,*], Jacqueline L.E. Tearle[†], Jianling Xie, Matt A. Govendir, Daryan Kempe, Jessica Mazalo, Alexander P. Drew, Feyza Colakoglu, Sarah K. Kummerfeld, Christopher G. Proud and Maté Biro[*]

[†] These authors contributed equally to this work

[*] Correspondence: s.tay@unsw.edu.au (SST) and m.biro@unsw.edu.au (MB)

SUPPLEMENTARY INFORMATION

SUPPLEMENTARY FIGURES

Fig. S1

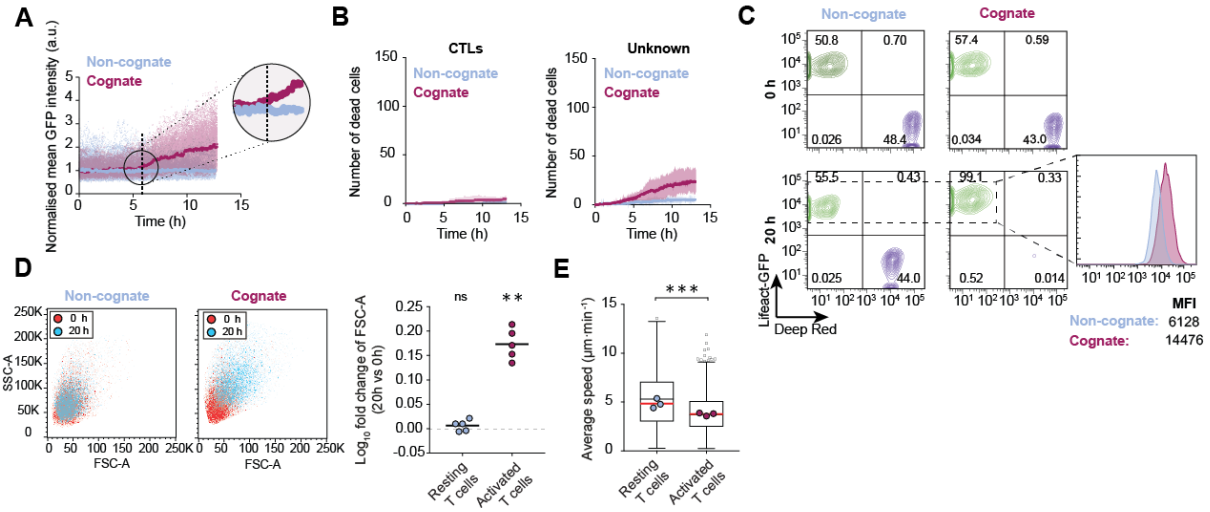

Figure S1. Determining time of activation, size and granularity in LGO1 cell populations.

A Time-series of normalised distributions of mean GFP intensities of LGO1 cells interacting with cognate (n=722 T cells, red) or non-cognate (n=650 T cells, blue) EL-4. Medians per timepoint shown as thick lines. Time of divergence/activation determined by means of a non-parametric right-tailed Wilcoxon rank sum test ($p < 0.0014$), indicated by dashed black line.

B Number of tracked PI surfaces ascribed to LGO1 effector CTLs (left) or that could not be ascribed (right) when LGO1 were co-embedded in a 1:1 ratio with cognate (red) or non-cognate (blue) EL-4 tumours in 3D collagen matrices as describes in Fig. 1E. Data points indicate the mean of pooled data from 3 independent experiments; error bars indicate 95% confidence interval.

C Flow cytometric analysis depicting intensities of Lifeact-GFP (green) in LGO1 cells and CellTracker Deep Red-stained EL-4 tumour cells (purple) in non-cognate (left) and cognate (right) contexts at 0h (top) and following 20 h of co-culture (bottom). Histogram overlays illustrates the shift in GFP fluorescence intensity when LGO1 cells are incubated with non-cognate (blue) and cognate (red) EL-4 cells.

D **Left and Middle:** Forward (FSC-A) and side (SSC-A) scatter plots of LGO1 cells incubated with non-cognate (left) and cognate (middle) EL-4 tumour cells, at 0h and 20h of incubation as indicated.

Right: Log10 fold change in FSC-A of LGO1 cells after 20h of incubation with non-cognate (resting T cells) and cognate (activated T cells) EL-4 tumour cells relative to the FSC-A of the corresponding T cell population at 0h. Bar: mean of pooled data from 5 independent experiments (data points). ns: $p > 0.05$ and ** $p < 0.01$ by one sample T test compared with a hypothetical test value of 0 (dashed line) (right).

E Average speeds of LGO1 cells imaged and tracked in 3D collagen matrices following a 20-hour incubation with non-cognate EL-4 cells (resting T cells: n= 4393) or cognate EL-4 cells (activated T cells: n=3702). Pooled data from 3 independent experiments; data points: average for each experiment; red bar: mean; box-whiskers: medians and quartiles, with outliers outside whiskers. *** $p < 0.001$ by Mann-Whitney U test.

Fig. S2

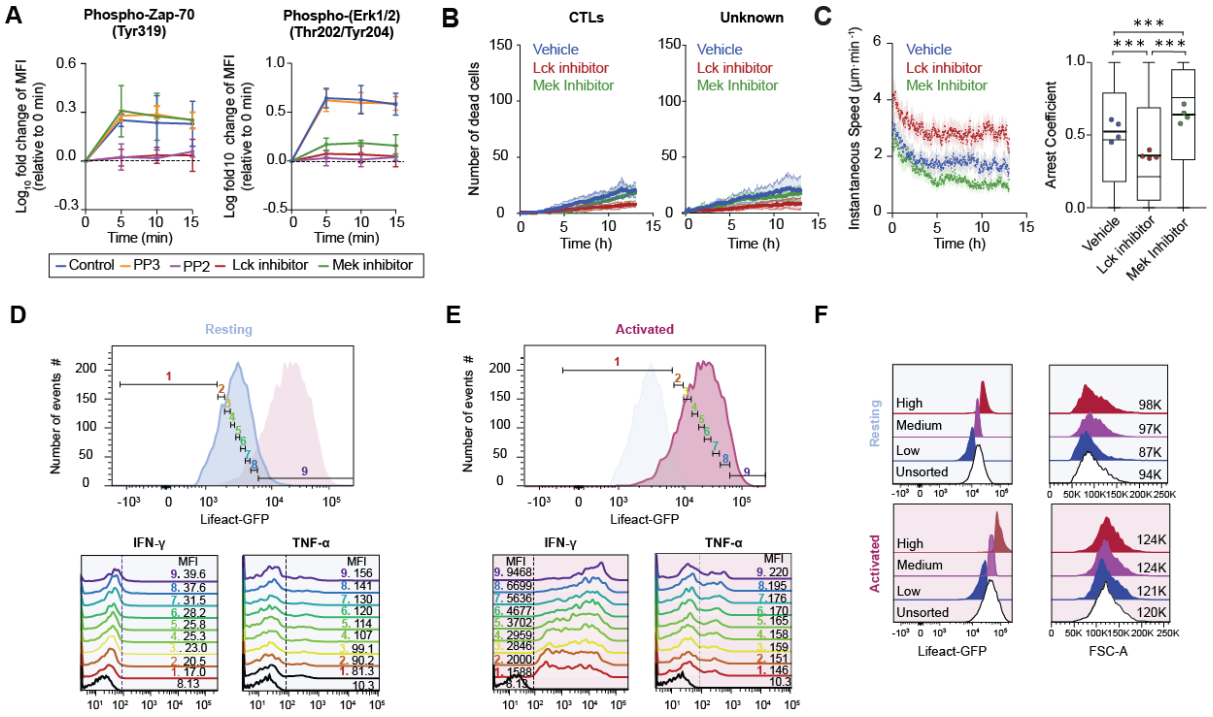

Figure S2. Lifeact-GFP enhanced fluorescent is TCR signalling mediated and it is correlated with the expression of IFN-γ and TNF-α in LGO1 cells

A Log_{10} fold change of the mean fluorescence intensity (MFI) of phospho-Zap-70 (Tyr319) (left) or phospho-Erk1/2 (Thr202/Tyr204) (right) staining intensities relative to resting values at 0 min (pre-activation) in LGO1 cells stimulated by streptavidin beads coated with cognate H-2K^b/SIINFEKL pMHC for 5, 10 and 15 min in the presence of Src-family kinase inhibitors PP2 (10μM) or PP3 (10μM), 10μM Lck inhibitor or 5μM Mek 1/2 inhibitor. Data points: mean from 3 independent experiments; error bars: range.

B Number of tracked PI surfaces ascribed to CTLs (left) or that could not be ascribed (right), when LGO1 cells were co-embedded in a 1:1 ratio with cognate EL-4 tumour targets in 3D collagen matrices treated with the indicated inhibitors or vehicle control as indicated in **Fig. 2B**. Data points indicate the mean of pooled data from 3 independent experiments; error bars indicate 95% confidence interval.

C **Left:** Instantaneous speed of LGO1 cells co-embedded with cognate EL4 tumour cells in 3D collagen matrices, treated with indicated inhibitors or vehicle control and tracked following live-cell imaging. Data points: population mean instantaneous speed from 453 vehicle, 340 Lck inhibitor and 268 Mek 1/2 inhibitor-treated T cells; error bars: 95% confidence interval; representative of 4 independent experiments.

Right: Distribution of the arrest coefficient of LGO1 cells co-embedded with cognate EL4 tumour cells and treated with inhibitors or control as indicated (Control: n=4686, Lck inhibitor: n= 4594, Mek inhibitor: n= 3666 T cells). Data points: means; box-whiskers: medians and quartiles from pooled data of 4 independent experiments; thick bars: mean of pooled data; *** $p < 0.001$ by Kruskal-Wallis test followed by Dunn's multiple comparison test.

D **Top:** Representative histograms showing the designation of 9 gates based on GFP mean fluorescence intensity in resting LGO1 cells after 20h of incubation with the non-cognate tumour cells.

Bottom: Mean fluorescence intensities (MFI) of IFN-γ (left) and TNF-α (right) for each gate as indicated for resting LGO1 cells. Representative plots from 4 independent experiments.

E **Top:** Representative histograms showing the designation of 9 gates based on GFP mean fluorescence intensity in activated LGO1 cells after 20h of incubation with the cognate tumour cells.

Bottom: Mean fluorescence intensities (MFI) of IFN-γ (left) and TNF-α (right) for each gate as indicated in activated LGO1 cells. Representative plots from 4 independent experiments.

F **Left:** Fluorescence intensity of sorted LGO1 populations distinguished by GFP intensity after co-incubation for 20h with non-cognate (resting, top) or cognate (activated, bottom) EL4 tumour cells. An unsorted population was established as a control. Representative plots from 3 independent experiments.

Right: Forward scatter area (FSC-A) histograms of LGO1 cells after cell sorting from the co-culture for 20h with non-cognate (resting, top) or cognate (activated, bottom) EL4 tumour cells. Representative plots from 3 independent experiments.

Fig. S3

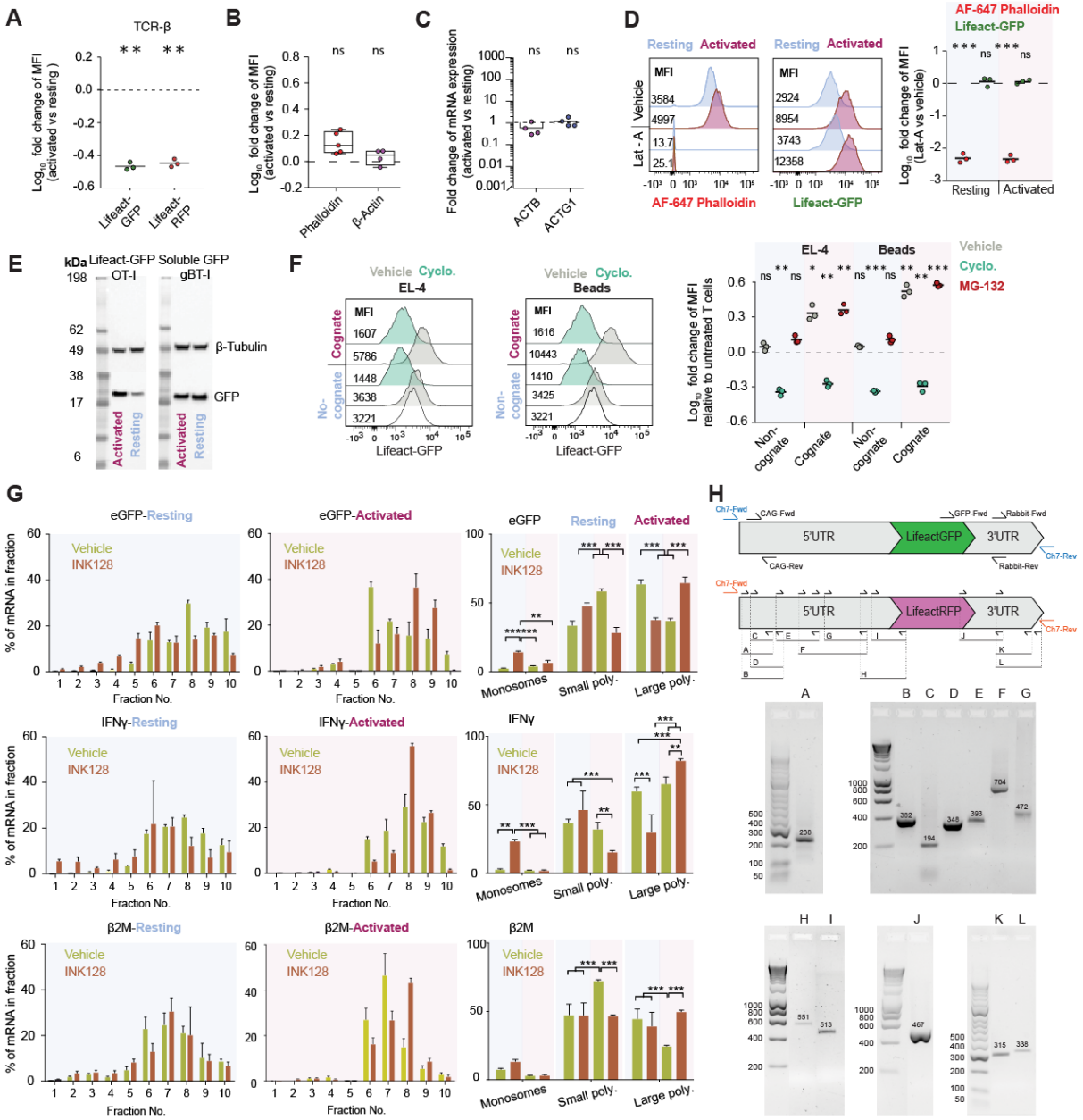

Figure S3. Gain in Lifeact-GFP fluorescence is not related to F-actin polarization and it is regulated at the translational level.

A Log_{10} fold change of the mean fluorescence intensity (MFI) of TCR-Vα expression in polyclonal effector T cells from the Lifeact-GFP or Lifeact-RFP mice stimulated for 20h with streptavidin beads coated with biotinylated CD3/CD28 antibodies (activated) or beads coated with biotinylated IgG isotype control antibodies (resting). Data points are from independent experiments, bars represent the mean. ** p <0.01 by one sample T test compared with a hypothetical test value of 0 (dashed line).

B Log_{10} fold change of the mean fluorescence intensity (MFI) of phalloidin and anti-β-actin staining in activated LGO1 cells relative to resting cells. LGO1 cells were pre-incubated

for 20h with cognate (Activated) or non-cognate (Resting) EL4 tumour cells respectively as measured by flow cytometry. Data points: 4 independent experiments; box-whiskers: medians and quartiles of the pooled set. ns: $p > 0.05$ by one sample T test compared with a hypothetical test value of 0 (dashed line).

C Fold change of mRNA expression via quantitative real-time PCR analysis of ACTB and ACTG1 in LGO1 cells sorted from cognate (activated) versus non-cognate (resting) EL4 tumour cells after 20h of incubation. Expression levels normalised to housekeeping genes RPL13A and β2M. Data points: 4 independent experiments; bars: mean. ns: $p > 0.05$ by one sample T test compared with a hypothetical test value of 0 (dashed line).

D **Left and Middle:** Representative histograms showing the mean fluorescent intensities (MFI) of phalloidin conjugated with Alexa Fluor 647 (AF-647) staining (Left) or Lifeact-eGFP (Middle) in activated or resting LGO1 cells treated with vehicle or 1μM latrunculin A (Lat-A). LGO1 cells were pre-incubated for 20h with cognate (activated) or non-cognate EL4 (resting) tumour cells.

Right: Log_{10} fold change of MFI of phalloidin staining or Lifeact-EGFP in activated or resting LGO1 cells treated with LatA compared to vehicle. Data points: 3 independent experiments; bars: mean. ns: $p > 0.05$ and *** $p < 0.001$ by one sample T test compared with a hypothetical test value of 0 (dash line).

E Western Blot showing protein levels of β-tubulin (loading control) and eGFP in sorted LGO1 or UBI-GFP.gBT-I cells after 20h of incubation with cognate (activated) or non-cognate (resting) EL4 tumour cells.

F **Left and Middle:** Representative histograms showing the mean fluorescent intensities (MFI) of Lifeact-eGFP in LGO1 cells pre-treated with cycloheximide 10μM (Cyclo.) or vehicle and then stimulated for 20h with cognate or non-cognate EL4 cells (Left) or with cognate (H-2K^b/SIINFEKL) or non-cognate (H-2K^b/RGYVYQGL) beads (Middle).

Right: Log_{10} fold change of Lifeact-GFP mean fluorescence (MFI) in LGO1 cells pre-treated with Cyclo. 10μM, MG-132 5μM or vehicle in the presence of cognate or non-cognate EL4 cells or with beads. The MFI is relative to the Lifeact-eGFP fluorescence of untreated resting LGO1 cells, as measured by flow cytometry. Data points: 3 independent experiments; bars indicate the mean of the pooled set. ns: $p > 0.05$, * $p < 0.05$, ** $p < 0.01$and *** $p < 0.001$ by one sample T test compared with a hypothetical test value of 0 (dashed line).

G Distribution of eGFP, IFNγ and B2M messages across monosomes, small and large polysomes quantified by RT-qPCR. **Left and Middle:** Percentage distribution of mRNA

expression of eGFP (Top), INF-γ (Centre) and β2 microglobulin (Bottom) for each polysome fraction in sorted LGO1 cells pre-treated with INK128 or vehicle and then incubated with non-cognate (Resting, left) or cognate (Activated, middle) EL-4 tumour cells. **Right:** Percentage distribution of mRNA expression of eGFP (Top), INF-γ (Centre) and β2 macroglobulin (Bottom) in monosomes (fractions 1-4), small polysomes (fractions 5 to 7) and large polysomes (fractions 8 to 10) from sorted LGO1 cells pre-treated with INK128 or vehicle and then incubated with cognate (activated) or non-cognate (resting) EL-4 tumour cells. Data are means ± S.D., n = 3. *: $0.01 \leq p < 0.05$; **: $0.001 \leq p < 0.01$; ***: $p < 0.001$ (Two-way ANOVA)

H Amplification and/or sequencing of flanking regions of the Lifeact-GFP (Top) and Lifeact-mRFPruby (Bottom) transgenes confirms that the 5' and 3' UTRs are identical in the two transgenic mice. Indicated primers are reported in Methods.

Fig. S4

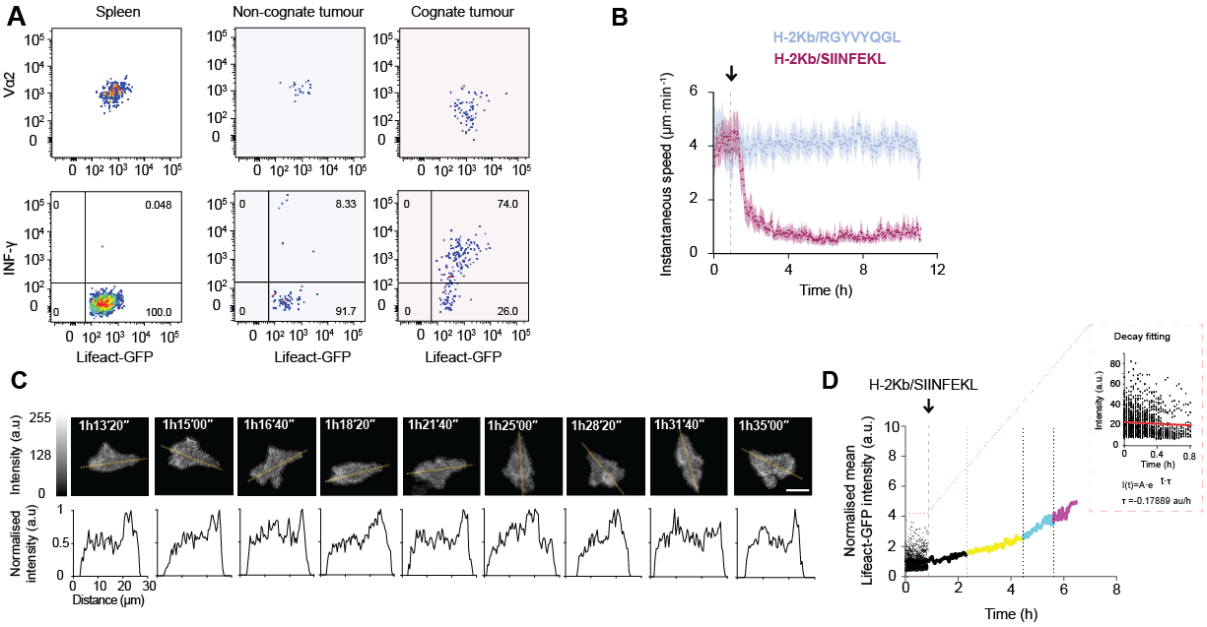

Figure S4. Enhanced Lifeact-GFP fluorescence can be monitored *in-vivo* and it is identifiable at a single-cell imaging.

A **Top:** Representative flow cytometry plots showing the expression of Lifeact-GFP and TCR-Vα2 in effector LGO1 cells isolated from spleen (left), non-cognate (centre) or cognate tumours after 24h post-T cell transfer.

Bottom: Representative flow cytometry plots showing the expression of Lifeact-GFP and IFN-γ in effector LGO1 cells isolated from spleen (left), non-cognate (centre) or cognate tumours after 24h post-T cell transfer.

B Instantaneous speeds of LGO1 cells embedded in 3D collagen matrix. After ~1 h of imaging (dashed line) either cognate (H-2K^b/SIINFEKL, n=832 T cells) or non-cognate (H-2K^b/RGYVYQGL, n=1614 T cells) monomeric pMHC was added to the bathing medium as indicated. Data points: population mean; error bars: 95% confidence interval.

C Top: maximum intensity projections of F-actin localisation (Lifeact-EGFP) in an LGO1 cell embedded in 3D collagen matrix following acute addition of monomeric non-cognate pMHC at 0h. Orange lines: region of intensity linescan analysis (bottom).

D Main: Normalised GFP mean fluorescence intensity (MFI) before treatment (black data points, all cells) and representative cell after acute addition of cognate pMHC (dashed lined) (black, yellow, cyan, magenta solid curve). Black, yellow, cyan and magenta indicate regimes of the T cell activation confidence levels.

Inset: GFP intensity distributions before addition of cognate pMHC re-aligned such that all tracks initiate at 0h prior to photo-bleaching correction (black triangles). Mono-exponential decay function (red line) fitted to data set and subsequently used for normalisation of data in Main plot.

SUPPLEMENTARY MOVIES

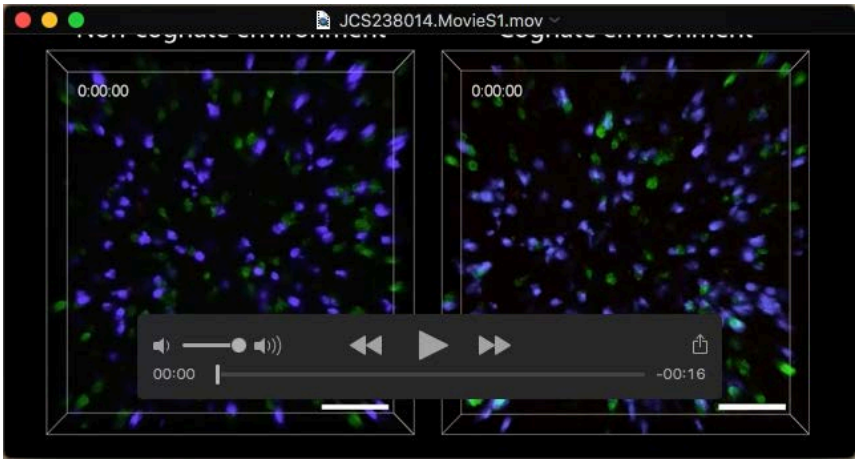

Movie 1 – Search and kill assay using cognate targets

Live-cell imaging of LGO1 cells (green) co-embedded with non-cognate (left) or cognate (right) EL-4 tumour cells (blue) in a 3D collagen matrix over 12 h. Killed cells appear in pink (propidium iodide uptake). Time in h:min:s. Scale bar: 100µm

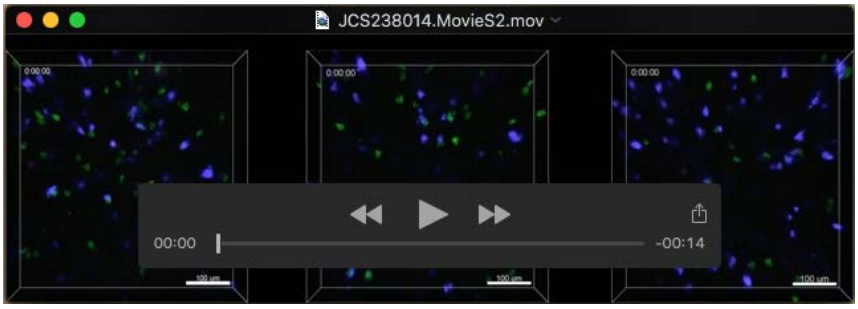

Movie 2 – Search and kill assays of cognate targets in the presence of Lck and Mek 1/2 inhibition

Live-cell imaging of LGO1 cells (green) co-embedded with cognate EL-4 tumour cells (blue) in a 3D collagen matrix over 12 h in the presence of vehicle (left), 10 µM Lck inhibitor (middle) and 5 µM Mek 1/2 inhibitor (right). Killed cells appear in pink (propidium iodide uptake). Time in h:min:s. Scale bar: 100µm

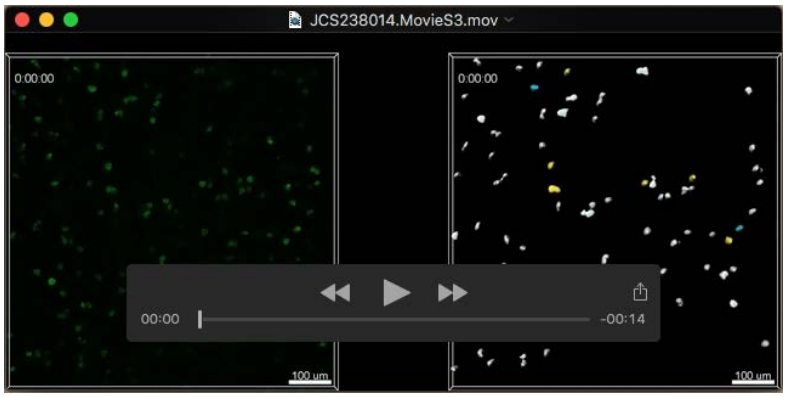

Movie 3 – Identification of activated T cells in 3D imaging data in a cognate environment

Live-cell imaging of LGO1 cells (raw fluorescence, left; coloured surface rendering, right) co-embedded with cognate EL-4 tumour cells (not shown) in a 3D collagen matrix over 12 h. Surfaces are coloured according to activation confidence level as described in **Figure 5A**: grey: indeterminate, yellow: low, cyan: medium, magenta: high. Time in h:min:s. Scale bar: 100µm

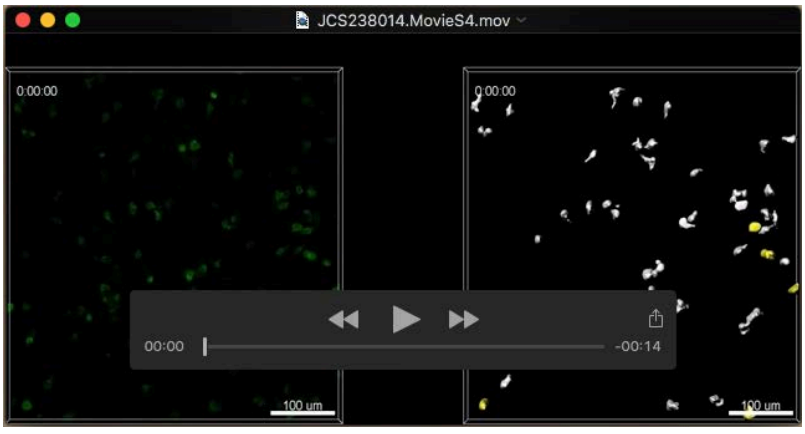

Movie 4 – Identification of T cells in 3D imaging data in a non-cognate environment

Live-cell imaging of LGO1 cells (raw fluorescence, left; coloured surface rendering, right) co-embedded with non-cognate EL-4 tumour cells (not shown) in a 3D collagen matrix over 12 h. Surfaces coloured according to activation confidence level as described in **Fig. 5A**: grey: indeterminate, yellow: low, cyan: medium, magenta: high. Time in h:min:s. Scale bar: 100µm

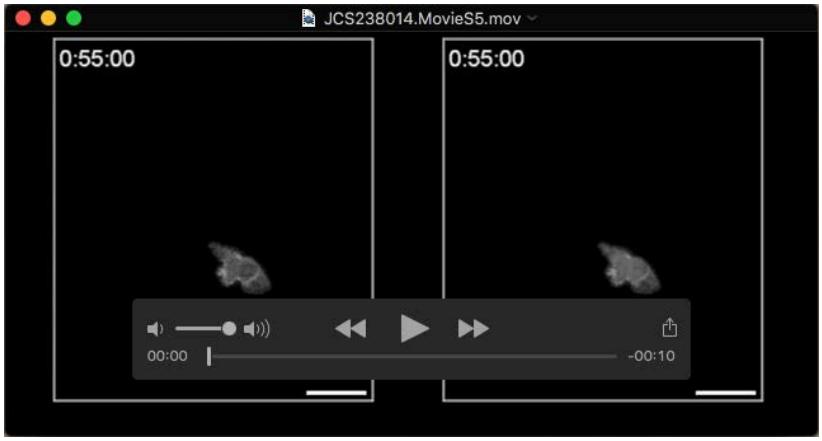

Movie 5 – Live analysis of single T cell activation

Live-cell imaging of an LGO1 cell (raw fluorescence, left; transparent coloured surface rendering, right) migrating in a 3D collagen matrix following acute addition of monomeric cognate pMHC molecules (t=0h). Surfaces coloured according to activation confidence level: grey: indeterminate, yellow: low, cyan: medium, magenta: high. Time in h:min:s. Scale bar: 10 µm.